ISSN 1064-2269, Journal of Communications Technology and Electronics, 2009, Vol. 54, No. 1, pp. 1–26. © Pleiades Publishing, Inc., 2009.
Original Russian Text © I.Ya. Immoreev, 2009, published in Radiotekhnika i Elektronika, 2009, Vol. 54, No. 1, pp. 5–31.

REVIEW

Ultrawideband Radars: Features and Capabilities

I. Ya. Immoreev

Received April 10, 2008

Abstract—Features of ultrawideband (UWB) radars, which radiate signals whose spatial duration is substantially smaller than the antenna dimensions and/or the longitudinal dimension of the illuminated target, are analyzed. It is shown that, during the radar observation of the target, this signal changes its shape several times and enters the radar receiver as an unknown signal. In many cases, this circumstance prohibits application of the traditional theory for the design of UWB radars. Methods for calculating the characteristics of UWB radars on the basis of the energy approach are proposed. Examples of engineering and circuit designs of several UWB radars are presented. Possible lines of development of the technology and technique of such radars are considered.

PACS numbers: 07.57.-c, 84.40.Xb

DOI: 10.1134/S106422690901001X

INTRODUCTION

The interest in ultrawideband systems that has grown in the last decade is primarily stimulated by the capabilities of such systems to increase the amount of transmitted and received information. The rapid growth of data transmission in the modern world makes this problem very important. As was shown by Shannon [1], the potential capacity of a data channel (the amount of information transferred per unit time) is directly proportional to absolute frequency bandwidth Δf of this channel. Therefore, one of the ways to further develop information systems is expansion of the absolute frequency bandwidth, which is realized via passage to UWB signals.[1]

The first definition of UWB signals and systems was introduced in 1990 by the US Defense Advanced Research Program Agency (DARPA) [2]. According to this definition, UWB signals and systems are those satisfying the inequality $0.25 < \eta \le 1$, where parameter η is the fractional bandwidth:[2]

$$\eta = \frac{f_u - f_l}{f_u + f_l},$$

where f_u and f_l are the upper and lower limits of the frequency band. This definition is widely used in Russian and foreign publications.

Another definition appeared in 2002. The US Federal Communications Commission (FCC) adopted the FCC 02-48 First Report and Order [3] (supplemented with the FCC 04-285 Second Report and Order and Second Memorandum Opinion and Order in 2004 [4]), according to which UWB signals and systems possess at least one of the following characteristics:

(i) The spectrum width of radiated signals $f_u - f_l$, (where f_u and f_l are determined at a level of –10 dB relative to the spectrum maximum) is at least 500 MHz.

(ii) The ratio of spectrum width $f_u - f_l$ (at a level of –10 dB) and the spectrum's center frequency $(f_u + f_l)/2$ (the relative bandwidth) is no less than 0.2.

This definition is used for classification of prototypes and commercial types of electronic equipment as UWB systems.

As shown in several publications devoted to investigation of UWB systems [5–14], in such systems, the processes of radiation, reception, and processing of radio signals are substantially different from similar processes in narrowband systems. These differences are especially pronounced in such practically important cases when the spatial duration of a UWB signal becomes substantially less than the dimensions of the antenna and/or the longitudinal dimension of the illuminated target.

Let us designate the spatial duration of a signal as $c\tau$, where c is the velocity of light and τ is the signal duration. (In the case of the intrapulse modulation, parameter τ determines the width of the signal's autocorrelation function and $c\tau$ is the spatial duration of the signal with consideration for the subsequent matched processing.)

[1] Ultrawideband signals have a very small duration, which in fact allows an increase in the amount of information transferred over a data channel per unit time. Therefore, it would be logical to call these signals and systems ultrashort-pulse signals and systems; this term is used by some authors [15]. However, the term ultrawideband is widely used in world scientific literature and the application of other terms is not beneficial.

[2] The same parameter multiplied by 2 is called the relative bandwidth.

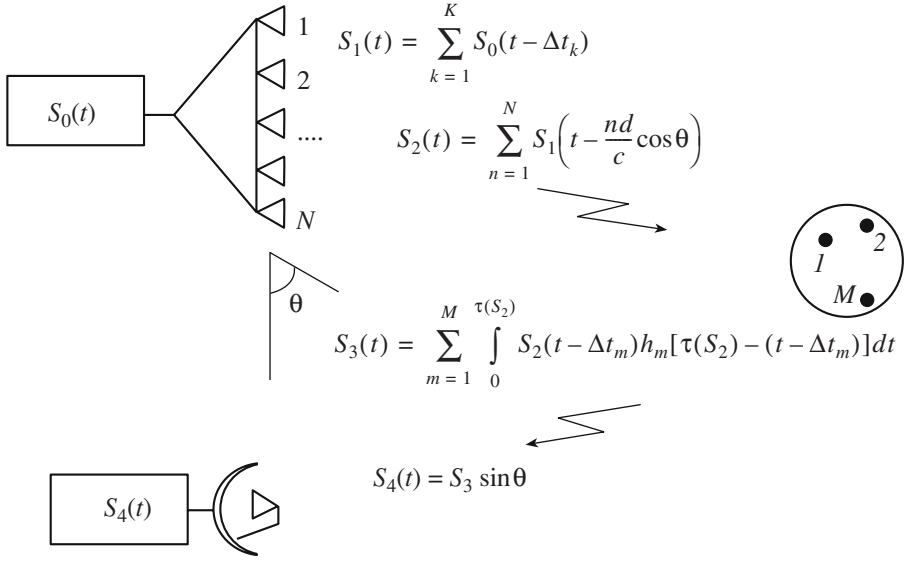

Fig. 1. Successive variations in the shape of a UWB signal during radar observation of a target.

Traditional narrowband signals practically always satisfy the inequality $c\tau \gg L$, where L is the antenna dimension and/or the longitudinal dimension of the illuminated target. The most typical inequality for the UWB signals, which have very small durations, is $c\tau \ll L$. As will be shown below, if this inequality is fulfilled, the system acquires a new important feature: The signal shape[3] substantially varies during radiation, reflection from the target, and reception. Exactly this feature causes differences between the UWB systems and systems of other types and changes the approach to the design of such systems; therefore, this feature is worthy of a special analysis.

In this paper, we consider the UWB systems satisfying the inequality $c\tau \ll L$, analyze the factors that cause variations in the signal shape under the conditions of this inequality, study the main features arising in the UWB systems in this case, and propose some methods for calculation and design of such UWB systems.

1. VARIATIONS IN THE SHAPE OF A UWB SIGNAL DURING RADAR OBSERVATION: A GENERAL APPROACH

Let us consider the factors that cause variations in shape S of a UWB signal during radar observation of a target (Fig. 1). In this simplified scheme, a multichannel antenna in the form of an array of N radiators is used for radiation and the receiver is connected to a single-channel (horn or reflector) antenna.

Let us begin with the processes occurring in one radiator of the array. The signal from the transmitter, which has the form of a current pulse with shape $S_0(t)$ and duration τ, enters the input of a radiator with length L. This current pulse occupies part $c_0\tau$ of the radiator length, where c_0 is the velocity of travel of charges in the radiator's material. For the considered UWB signals, $c_0\tau \ll L$. Therefore, the aperture of this radiator is nonsimultaneously excited by the traveling current pulse, while the excitation process extends in time and terminates when the current pulse completes its travel over the radiator. During this travel, several electromagnetic pulses (rather than one) are formed in the space. Let the number of pulses be K and the time interval between the pulses be Δt_k. This process is detailed in Section 2. The excited field pulses form a radiated signal whose shape $S_1(t)$ differs from shape $S_0(t)$ of the current pulse. Intervals Δt_k depend on radiator length L. Since radiator's visible length L depends on observation angle θ, signal shape $S_1(t)$ is likewise a function of this angle.

However, current pulse $S_0(t)$ enters all N array radiators (rather than one), which simultaneously radiate signal $S_1(t)$. In the directions that deviate from the normal to the antenna aperture, there are time delays between the field pulses arriving from different radiators at some observation point in the far zone. For adjacent radiators, this delay is $(d/c)\cos\theta$, where d is the spacing between the radiators. Summation of N delayed signals $S_1(t)$ forms a signal with shape $S_2(t)$, which differs from shape $S_1(t)$. This shape is different for different observation angles θ and, sometimes, may be very complex.

The next variation in the shape of the UWB signal occurs during reflection of this signal from M local scattering centers (specular points) of the illuminated object, which are arbitrarily distributed along object

[3] Here and below, the signal shape is considered to mean the time dependence of a signal carrier (voltage, current, electromagnetic field, etc.).

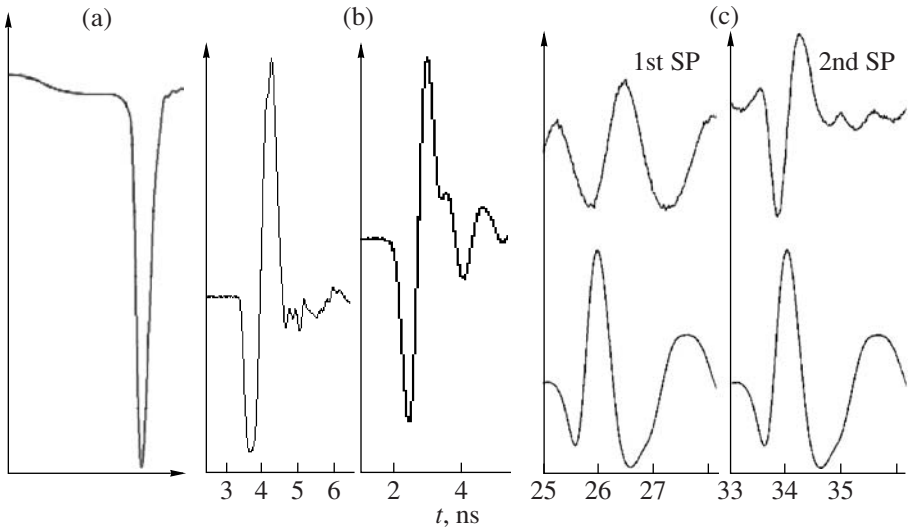

Fig. 2. Examples of real UWB signals: (a) the signal of the transmitter, (b) radiated signals, and (c) signals reflected from different specular points (SPs) of the target. The radiated signal is shown at the bottom, and the reflected signal is shown at the top.

length L_1. Signal $S_2(t)$ is reflected from each of these centers and acquires different delays Δt_m (whose values depend on the radial distances between the centers), different intensities (whose values depend on the reflection characteristics of each center), and different polarities (which depend on the object material). The sum of signals $S_2(t)$ reflected from local scattering centers form signal $S_3(t)$ whose shape differs from shape $S_2(t)$. This shape depends also on impulse responses h_m of local centers, which may serve as frequency filters for the signal. The signal reflected from a complex object is called the target pattern. The entire pattern is formed in time $T = 2L_1/c$, and the shape of this pattern is a function of the object's observation angle.

Subsequent variations in the shape of the UWB signal occur during reception (see Section 5 for details). These variations are caused by the dependence of the directional pattern of the receiving antenna on shape $S_3(t)$ of the field pulse reflected from the object and incident onto the antenna and on the time shifts of the current pulses induced by field $S_3(t)$ on different parts of the receiving antenna, whose length is substantially larger than the spatial duration of incident signal $S_3(t)$. The voltage across the load of the receiving antenna has shape $S_4(t)$, which differs from shape $S_3(t)$ of the field.

In addition, variations in the shape of the UWB signal, which occur during propagation of this signal to the object and backward and which are caused by different values of attenuation of different segments of the signal spectrum in the atmosphere, should be taken into account. Thus, the receiver of a UWB radar receives a signal with an unknown shape. Figure 2 shows examples of real UWB signals obtained at different stages of radar observation.

The aforementioned variations in the signal shape result in some difficulties during estimation of parameters of UWB radars.

For example, the antenna pattern, which is defined as the dependence of the electromagnetic-field amplitude on angular coordinates, becomes time-dependent and changes its position in space during the passage of the current pulse over the radiating antenna or during the passage of the field pulse over the receiving antenna. (This issue will be analyzed in more detail in Sections 3 and 4.)

An unknown shape of the received signal prohibits processing of the signal with a correlator using a reference signal or a matched filter. Such processing requires application of methods that allow obtainment of the maximum value of the signal-to-noise ratio during processing of a signal with an unknown shape (see Section 5).

The complex shape of the field incident onto the receiving antenna (signal $S_3(t)$ causes difficulties in determining the target's radar cross section (RCS) because the signal values that must be taken as the amplitudes of the electromagnetic field at the illuminated object and at the reception point are unknown (see Section 6 for details).

Let us consider in more detail some issues related to the aforementioned variations in the signal shape.[4]

[4] In the literature devoted to the analysis of UWB systems, such variations in the signal shape are sometimes incorrectly termed signal distortions. In this regard, we should note that the aforementioned variations in the shape of the UWB signal are the results of objective mechanisms, while distortions should be considered variations caused by imperfect characteristics of the equipment. We can refer to the well-known *Russian Language Dictionary* by S.I. Ozhegov (Moscow, Russkii Yazyk, 1985), where the term *variation* is defined as a correction or change that changes something preceding, while the term *distortion* is defined as incorrectness or error.

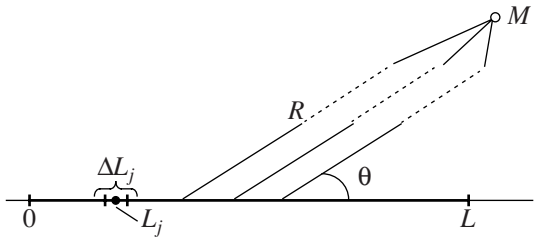

Fig. 3. Model of one dipole arm.

2. VARIATIONS IN THE SIGNAL SHAPE DURING RADIATION

The processes lying behind excitation of the antenna and radiation of the signal in the case of $c\tau \ll L$ are considered in many Russian and foreign publications for both series excitation of the entire aperture (in traveling-wave antennas) and parallel excitation (in aperture antennas). In the literature, excitation under the above condition is often called nonstationary (time-dependent) excitation. A review of these studies is presented in [16].

In these studies, rigorous solutions to the exterior electromagnetic problem were obtained. These solutions can be used to determine the field generated by the antenna in the far zone for a specified shape of the exciting current at $c\tau \ll L$. However, the obtained solutions are cumbersome, which hampers understanding of physical processes occurring in the antenna. Therefore, we consider the simplest model of the radiator of a UWB signal in the form of a linear antenna (for example, a dipole arm) and give a physical interpretation of processes in this antenna in order to understand why shape $S_1(t)$ of the radiated field is substantially different from shape $S_0(t)$ of the exciting current.

We will use of the antenna model presented in [17] (Fig. 3). Let us divide the antenna with length L into elementary radiators with length ΔL. In the figure, the following designations are used: ΔL_j is the jth elementary radiator, L_j is the coordinate of this radiator, R is the distance to observation point M, and θ is the angle between the direction toward the observation point and the aperture plane. Current pulse $i(t)$ arrives at point O, propagates along the antenna, and sequentially excites its aperture.

The electromagnetic field of an elementary radiator is related to the charge motion in the radiator via the following well-known relationship [18]:

$$E(t) = \frac{q}{4\pi\varepsilon}\left[\frac{1}{c^2}\frac{d^2\vec{e}_r}{dt^2}\right],$$

where q is the charge and $\vec{e}_r$ is the unit vector of the charge.

Since the current is $i(t) = dq/dt$, acceleration of chargers in an elementary radiator generates a field that is proportional to the first derivative of the current.

After the arrival of a current pulse at point O, the first elementary radiator is excited. In time R/c, an electromagnetic field is generated at point M in the far zone. This field can be expressed as [16]

$$E_1(t,\theta) = \frac{Z_0\sin\theta}{4\pi c}\frac{1}{R}\frac{d}{dt} \times\left[i\left(t-\frac{L_1}{c_0}-\frac{R-L_1\cos\theta}{c}\right)\right]\Delta L, \quad (1)$$

where Z_0 is the wave impedance of free space and c_0 is the propagation speed of the signal in the radiator's wire. The second term in parentheses determines the signal delay in this wire, and the third term determines the signal delay in space.

In time $\Delta L/c$, the current pulse excites the second elementary radiator and excites second electromagnetic field $E_2(t, \theta)$, which is described by an expression similar to (1) in which L_1 is replaced with L_2.

During its travel along the wire, the current pulse successively excites subsequent elementary radiators. In order to obtain a relatively simple physical picture of the processes occurring in the antenna, we introduce some simplifications that do not change the final result (which coincides with the results of the rigorous theory). Let us disregard loss in the antenna wire and assume that the delay in the wire is absent ($c_0 = c$). Let us assume also that the current pulses are not reflected from the antenna end but are totally radiated into the ambient space. This radiator is called a matched radiator.

In this case, the total far field of all elementary radiators has the form

$$E_\Sigma(t,\theta) = \frac{Z_0\sin\theta}{4\pi c}\frac{1}{R} \times\sum_{j=1}^{N}\frac{d}{dt}\left[i\left(t-\frac{L_j}{c}-\frac{R-L_j\cos\theta}{c}\right)\right]\Delta L. \quad (2)$$

Let us pass from discrete representation of the antenna to continuous representation by tending the length of an elementary radiator toward zero ($\Delta L \longrightarrow 0$) and tending number N of radiators toward infinity ($N \longrightarrow \infty$). Then, summation in (2) transforms into integration:

$$E_\Sigma(t,\theta) = \frac{Z_0\sin\theta}{4\pi c}\frac{1}{R} \times\int_0^L\frac{d}{dt}\left[i\left(t-\frac{L}{c}-\frac{R-L\cos\theta}{c}\right)\right]dL. \quad (3)$$

Expression (3) describes the electric component of the far electric field of an extended antenna excited from one end by an arbitrary current.

The field determined from expression (3) is formed with consideration for the delays of the current pulse in the wire and the field pulse in space. The expression in parentheses shows the current time with consideration for this delay. After calculating the derivative of this time with respect to dL, we can perform the following change of variables in (3) [19]:

$$dt = \frac{\cos\theta - 1}{c} dL.$$

As a result, we obtain the integral of a function derivative with respect to the integration variable. Such an integral is equal to the function itself. Then

$$E_\Sigma(t, \theta) = \frac{Z_0 \sin\theta}{4\pi R} \frac{1}{\cos\theta - 1}$$

$$\times \left[i\left(t - \frac{L}{c} - \frac{R - L\cos\theta}{c} \right) \right]_0^L = \frac{Z_0 \sin\theta}{4\pi R} \frac{1}{\cos\theta - 1} \quad (4)$$

$$\times \left[i\left(t - \frac{L}{c} - \frac{R - L\cos\theta}{c} \right) - i\left(t - \frac{R}{c} \right) \right].$$

This expression shows that, in the general case, the field generated by the antenna consists of two parts, negative and positive, which have different delays. It can readily be shown that the shape of each part of this field repeats the shape of the exciting current pulse.

Let us analyze the shape of the total antenna field by a particular example. We assume that the exciting current pulse is a Gaussian curve with unit amplitude (Fig. 4, curve *1*):

$$i(t) = \exp[-4(t/\tau)^2], \quad (5)$$

where τ is the pulse duration at a level of 0.5. The derivative of this pulse is a symmetric bipolar pulse (Fig. 4, curve *2*). Substituting (5) into (4), we obtain

$$E_\Sigma(t, \theta) = \frac{Z_0 \sin\theta}{4\pi R} \left[\frac{1}{\cos\theta - 1} \right.$$

$$\times \left\{ \exp\left[-4\left(\frac{t - \frac{L}{c} - \frac{R - L\cos\theta}{c}}{\tau} \right)^2 \right] \right. \quad (6)$$

$$\left. \left. - \exp\left[-4\left(\frac{t - R/c}{\tau} \right)^2 \right] \right\} \right].$$

It is seen from (6) that the shape of the total field depends on the relationship between antenna length L and spatial duration $c\tau$ of the exciting pulse. This shape depends also on observation angle θ.

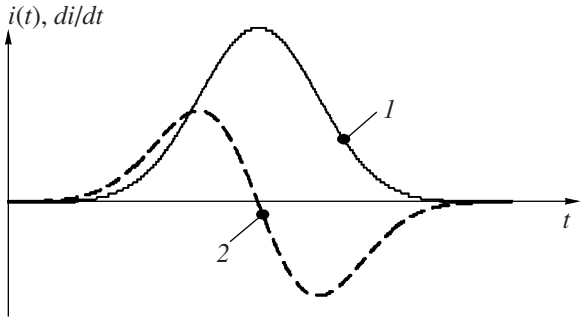

Fig. 4. Shapes of (curve *1*) current pulse $i(t)$ and (curve *2*) its derivative $di(t)/dt$.

Let us consider formation of field $E_\Sigma(t, \theta)$ from (6) at $c\tau \ll L$ by using the discrete antenna model shown in Fig. 3. The current pulse travels along the antenna and arrives at the elementary radiators with a delay. Therefore, the fields formed by these radiators at point M are shifted in time. Figure 5a uses a solid line to show these fields for the observation angle $\theta = 90°$. The fields have positive and negative half-waves with equal areas. Therefore, in the process of summation, these half-waves partially compensate each other. The degree of this compensation depends on the ratio of antenna length L and pulse duration $c\tau$. Complete compensation of fields starts at the time $t_c = \tau$. Only some portion of the fields of elementary radiators located near the excitation point and at the radiator end remains uncompensated (Fig. 5a, dashed line). Therefore, at $c\tau \ll L$, total radiator field $E_\Sigma(t, \tau, \theta)$ is separated into two individual fields, one of which is radiated at the instant when the pulse arrives at the antenna's excitation point, while the other field is radiated at the instant when the pulse reaches the antenna end. This process is sometimes treated as radiation from the excitation point and the antenna end.

As ratio $L/c\tau$ decreases, the time interval in which the fields compensate each other decreases relative to the duration of the field pulse. The interval between the field pulses shown in Fig. 5a decreases. Finally, at $c\tau \gg L$, compensation practically terminates and separated fields merge (Fig. 5b). Radiation occurs simultaneously from the entire aperture, and the shape of the total field approaches the shape of the derivative of the current pulse exciting the antenna.

Figure 6 shows total antenna fields $E_\Sigma(t, \tau, \theta)$ for $c\tau \ll L$ and different observation angles θ. It is seen from the figure that the shape of the total field pulse depends on the observation angle because the length of the projection of the antenna depends on the observation angle. The boundary angle at which the shape of the field pulse can be treated as two separate pulses

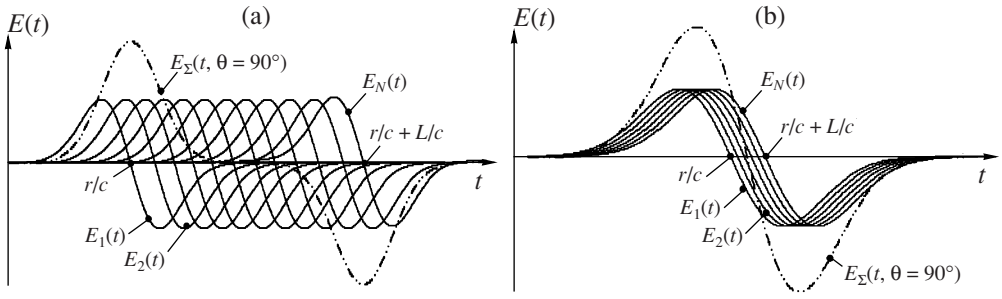

Fig. 5. Fields excited by elementary radiators at (a) $L/c\tau \gg 1$ and (b) $L/c\tau \ll 1$.

with different polarities is determined from the expression

$$\theta_b = \pi - \arccos[c\tau/L - 1].$$

Angle θ_b depends on the ratio $c\tau/L$. If $c\tau \gg 2L$, angle θ_b takes negative values. This means that the far field cannot be separated into two pulses at all observation angles θ.

Considered variations in the signal shape during radiation from one dipole arm are of a general nature. Depending on the type and design of the antenna, these variations may appear in different forms. The higher the antenna complexity, the higher the complexity of the shape of the field of radiated UWB pulses. If, for example, we change from one dipole arm to the entire dipole and take into account signal reflections from the ends, the pattern of the radiated field becomes far more complicated, a circumstance that hampers understanding of the processes governing formation of the total field. In antennas with a planar aperture, field pulses are excited also at the antenna's excitation point and at the edges [20]. In any case, if the condition $c\tau \ll L$ is satisfied, the antenna forms in the far zone a sequence of electromagnetic pulses separated by intervals depending on the antenna geometry. This sequence forms the radiated signal whose shape differs from the shape of the current pulse exciting the antenna.

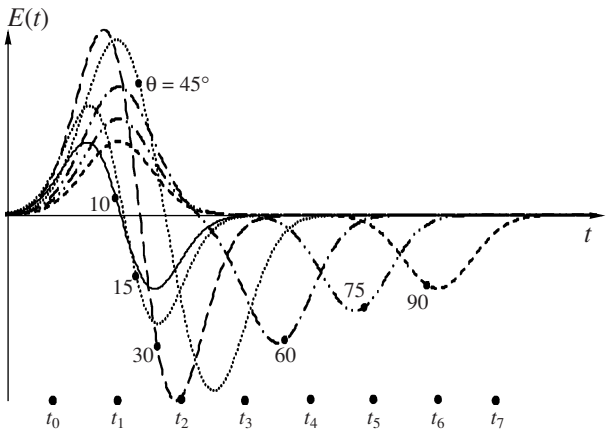

Fig. 6. Shapes of the field observed at different angles θ.

3. RADIATION PATTERN

Variations in the pulse shape with observation angle θ (Fig. 6) result in the time dependence of the field pattern. Let us demonstrate this dependence by the example of the aforementioned dipole excited by a Gaussian current pulse. The field excited by this pulse is described by expression (6). Field $E_\Sigma(t, \theta)$ depends on time, the angular direction, the shape of the exciting signal, and the antenna length. In our case, the shape of the exciting signal and the antenna length are fixed. In order to find the dependence of the field on the angular direction, we select several instants $t_0, t_1, t_2, t_3, \ldots$ in the interval during which the current pulse travels along the antenna and, by using expression (6), we consider field $E_\Sigma(t, \theta)$ as a function of θ at each of these instants. As a result, we obtain instantaneous patterns.

Figure 7 presents a family of instantaneous patterns obtained for $c\tau \ll L$.

As seen from the figure, the pattern maximum changes its direction during the time interval in which the field exists. At the initial instant, this maximum is directed practically along the antenna axis. As the pulse travels along the antenna, the pattern moves in space from the antenna axis toward the normal to this axis. During this motion, the pattern width and amplitude decrease. The behavior of the instantaneous patterns shown in Fig. 7 correlates with the results obtained in [21], where calculations were performed with the use of a rigorous model of a linear antenna.

In the case of a more complex (multipulse) shape of the radiated field, motion of the instantaneous pattern becomes more complicated, but the time dependence is retained.

This time dependence of the field pattern makes it unsuitable for calculation of the parameters of a radioengineering system because this dependence prohibits determination of such antenna parameters as the directivity factor and the beamwidth. In early publications (see, for example, [22]), other variants of construction

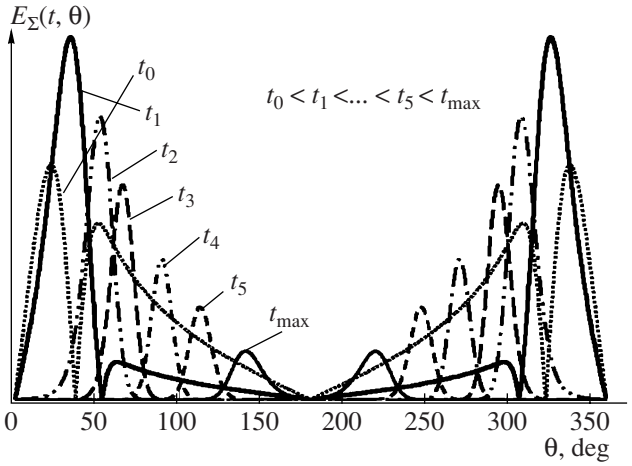

Fig. 7. Instantaneous patterns of an antenna with series excitation.

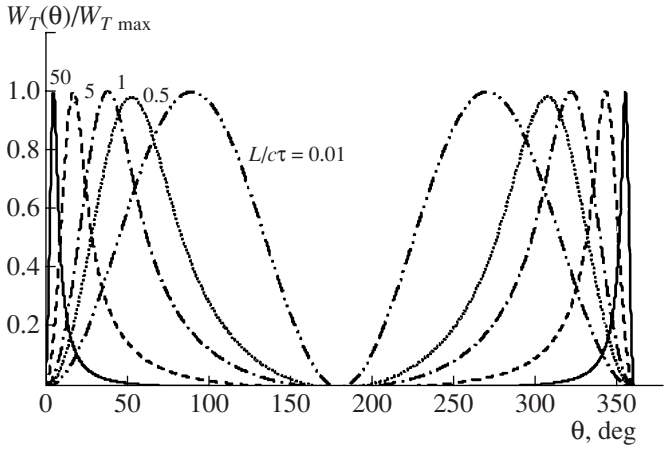

Fig. 8. One-dimensional (φ = const) energy patterns of an antenna with series excitation.

of the radiation pattern were described: namely, constructions based on the peak amplitude, the peak power, and the steepness. However, the energy pattern is most suitable for practical applications.

Spatial energy pattern $W_T(\theta, \varphi)$ is obtained via averaging of the power radiated in each angular direction in the time required for the pulse to travel along the antenna. This pattern describes the spatial distribution of the density of the radiated energy flux as a function of angles θ and φ [22, 23]:

$$W_T(\theta, \varphi) = \frac{1}{Z_0}\int_{-\infty}^{+\infty} E_\Sigma^2(\theta, \varphi, t)dt.$$

Infinite limits of integration in time allow application of this expression to current pulses with any shape and antennas of any length.

For comparison of the antenna characteristics, it is convenient to use the normalized energy pattern

$$W_{TN} = \frac{W_T(\theta, \varphi)}{W_{T\max}},$$

where the pattern value in the direction of the maximum radiation is calculated from the formula

$$W_{T\max} = \frac{1}{Z_0}\left[\int_{-\infty}^{+\infty} E_\Sigma^2(\theta, \varphi, t)dt\right]_{\max}.$$

Figure 8 presents normalized energy patterns for the example considered in this section at different values of ratio $L/c\tau$. If $c\tau \gg L$, the energy pattern coincides with the radiation pattern of a half-wave dipole. As ratio $L/c\tau$ increases, the pattern maximum deviates from the normal, and at $c\tau \ll L$, a linear antenna radiates along its axis. During these changes, the value of the pattern maximum increases and the pattern width decreases.

The directivity factor of an antenna radiating a UWB signal is defined as the ratio of the energy-flux density of the studied antenna in the direction of the maximum radiation ($W_{T\max}$) and the energy-flux density of an equivalent isotropic antenna (W_{T0}) at the same energy fed into the isotropic and studied antennas:

$$D_T = W_{T\max}/W_{T0}.$$

The total energy of the field radiated by the antenna through a sphere of radius R is

$$W = \frac{R^2}{Z_0}\int_0^{2\pi}\int_0^{\pi}\int_{-\infty}^{+\infty} E_\Sigma^2(\theta, \varphi, t)\sin\theta d\theta d\varphi dt.$$

By dividing this energy by the surface area of a sphere surrounding the antenna, we obtain the energy-flux density of the equivalent isotropic antenna:

$$W_{T0} = \frac{W}{4\pi R^2} = \frac{1}{4\pi Z_0} \times \int_0^{2\pi}\int_0^{\pi}\int_{-\infty}^{+\infty} E_\Sigma^2(\theta, \varphi, t)\sin\theta d\theta d\varphi dt.$$

The obtained expressions allow us to determine the energy directivity factor of the antenna:

$$D_T = 4\pi\frac{\left[\int_{-\infty}^{+\infty} E_\Sigma^2(\theta, \varphi, t)dt\right]_{\max}}{\int_0^{2\pi}\int_0^{\pi}\int_{-\infty}^{+\infty} E_\Sigma^2(\theta, \varphi, t)\sin\theta d\theta d\varphi dt}.$$

The antenna in the form of a dipole arm (Fig. 3), which was considered above, is an antenna with series excitation. If an antenna is simultaneously excited by a

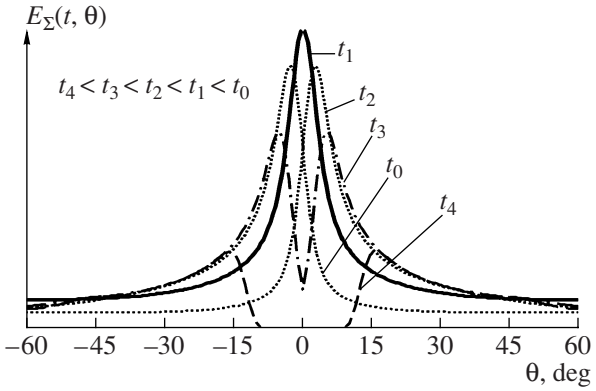

Fig. 9. Instantaneous patterns of an aperture antenna.

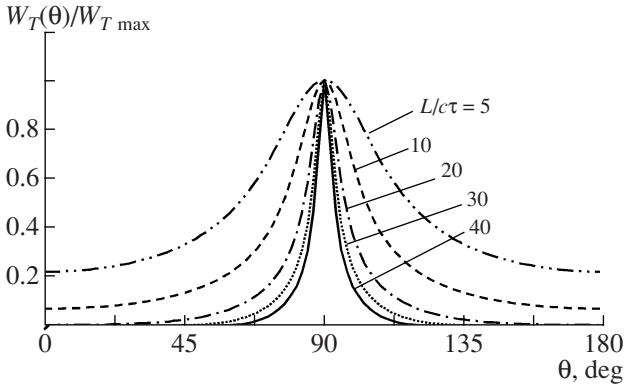

Fig. 10. Energy patterns of an aperture antenna.

short pulse (as in the case of an aperture antenna), the far fields generated at different angles likewise have different shapes. Instantaneous field patterns of such an antenna can be obtained from expression (4) or (6) upon removal of term L/c, which determines the delay of the current pulse for the travel time of this pulse along the aperture, from the expression in parentheses. These patterns are shown in Fig. 9 for different instants $t_0, t_1, t_2, t_3, \ldots$. Unlike the preceding case, the axis of the instantaneous pattern does not change its spatial orientation. However, during the time when the current pulse exists in the antenna, the pattern is separated into two diverging beams. A family of normalized energy patterns of an aperture antenna is shown in Fig. 10 for different values of ratio $L/c\tau$.

4. VARIATIONS IN THE SIGNAL SHAPE DURING RECEPTION AND FORMATION OF THE RECEPTION PATTERN

The shape of the total pulse of the radiated field varies with the observation angle (see Fig. 6). Hence, the shape of the field pulse incident onto the receiving antenna is a function of the angle between the receiving and transmitting antennas. As a result, the shape of the current pulse induced by this field in the receiving antenna and the shape of the voltage pulse at the antenna load, which is caused by the current pulse, depend on the mutual positions of these antennas. Hence, the pattern of the receiving antenna depends on these positions. Therefore, if $c\tau \ll L$, a UWB antenna has different patterns in the transmission and reception modes (unlike in the traditional theory used in the design of narrowband antennas).

In order to find the dependence of the shape of the received UWB signal on the mutual orientation of transmitting and receiving antennas, we consider Fig. 11, which depicts the positions of such antennas (dipoles with lengths L_T and L_R). The receiving antenna is placed at distance R from the transmitting antenna in the far zone of this antenna (at point M in Fig. 3). The load and the ends of the dipole are matched in the signal band and do not reflect the energy. The electric component of the field is radiated by the transmitting antenna toward the receiving antenna at angle θ_T between the line of the antenna aperture and the direction to the receiving antenna and is incident onto the receiving antenna at angle θ_R between the line of the antenna aperture and the direction to the transmitting antenna.

The electric component of the field radiated by one arm of the radiating dipole is described by formula (4), which, in view of new designations, takes the following form (the subscript of field E denotes the arm number):

$$E_1(t, \theta_T) = \frac{Z_0 \sin\theta_T}{4\pi R}\left[\frac{1}{\cos\theta_T - 1}\right.$$
$$\left.\times\left\{i\left(t - \frac{L_T}{c} - \frac{R - L_T\cos\theta_T}{c}\right) - i(t - R/c)\right\}\right].$$

The far electromagnetic field of the second dipole arm is determined from the expression

$$E_2(t, \theta_T) = \frac{Z_0 \sin\theta_T}{4\pi R}\left[\frac{1}{\cos\theta_T + 1}\right.$$
$$\left.\times\left\{i(t - R/c) - i\left(t - \frac{L_T}{c} - \frac{R + L_T\cos\theta_T}{c}\right)\right\}\right].$$

Then, the total field radiated by the dipole is

$$E_\Sigma(t, \theta_T) = E_1(t, \theta_T) + E_2(t, \theta_T)$$
$$= A_1 i\left(t - \frac{L_T}{c} - \frac{R - L_T\cos\theta_T}{c}\right) - A_1 i(t - R/c)$$
$$+ A_2 i(t - R/c) - A_2 i\left(t - \frac{L_T}{c} - \frac{R + L_T\cos\theta_T}{c}\right),$$

where A_1 and A_2 are the amplitude coefficients:

$$A_1 = \frac{Z_0 \sin\theta_T}{4\pi R(\cos\theta_T - 1)},$$

$$A_2 = \frac{Z_0 \sin\theta_T}{4\pi R(\cos\theta_T + 1)}.$$

Let us divide each arm of the receiving dipole into elementary segments dL_R. The electromotive force induced in an elementary segment is directly proportional to the projection of vector $E_\Sigma(t, \theta_T)$ of the electric component of the field incident onto this segment:

$$dE = E_\Sigma(t, \theta_T)\sin\theta dL_R.$$

In each elementary segment, this field generates the elementary current $dI = dE/Z$, where Z is the total impedance of the antenna circuit, which includes the radiation resistance and load impedance Z_L. To simplify the calculations, we assume that impedance Z is frequency-independent.

The elementary currents induced in each segment flow toward the load and toward the dipole ends. It was assumed above that the dipole ends are matched. Therefore, the part of these currents that flows toward the dipole ends creates the secondary radiation of the dipole. The currents flowing toward the load create a voltage drop across this load.

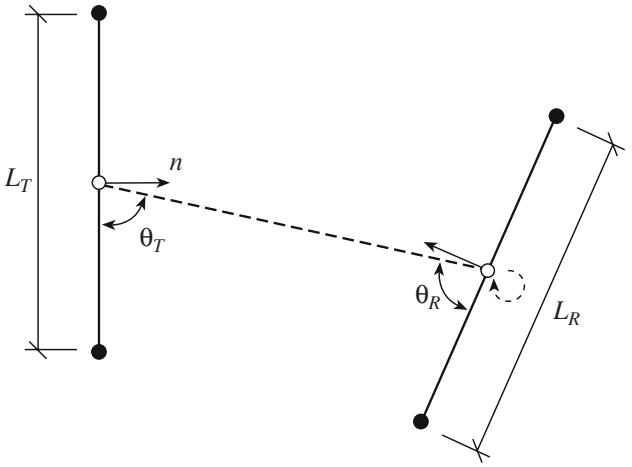

Fig. 11. Positions of transmitting and receiving antennas.

Note that, as in the case of radiation, the delay of the signal in the wire of the receiving dipole and in the space (if the field is incident at some angle to the dipole aperture) is

$$t_3 = \left(\frac{L_R + L_R\cos\theta_R}{c}\right).$$

In view of this delay, the total current flowing through the load of the receiving antenna is

$$I_\Sigma(t, \theta_T, \theta_R, L_T, L_R) = \int_0^{L_R} \left\{ \begin{array}{l} A_1 i\left(t - \frac{L_T}{c} - \frac{R - L_T\cos\theta_T}{c} + \frac{L_R}{c} + \frac{L_R\cos\theta_R}{c}\right) \\ \quad - A_1 i\left(t - R/c + \frac{L_R}{c} + \frac{L_R\cos\theta_R}{c}\right) \\ \quad + A_2 i\left(t - R/c + \frac{L_R}{c} + \frac{L_R\cos\theta_R}{c}\right) \\ - A_2 i\left(t - \frac{L_T}{c} - \frac{R + L_T\cos\theta_T}{c} + \frac{L_R}{c} + \frac{L_R\cos\theta_R}{c}\right) \end{array} \right\} dL_R. \quad (7)$$

The voltage across the load of the receiving dipole is

$$U_\Sigma(t, \theta_T, \theta_R, L_T, L_R) = I_\Sigma(t, \theta_T, \theta_R, L_T, L_R)Z_L.$$

Figure 12 shows the dependence of voltage $U_\Sigma(t, \theta, L)$ on angle θ_R. In calculations, it is assumed that the radiating dipole is excited by current pulse (5) with duration τ such that $c\tau \ll L_T$ and $L_R = L_T$. Angle θ_{TX} is 30° because, at this angle, the shape of the field pulse incident onto the receiving dipole is the closest to the shape of the derivative of the current pulse exciting the radiating dipole (see Fig. 4) and, as a consequence, the condition $c\tau \ll L_R$ is fulfilled for the receiving dipole.

It is clearly seen in Fig. 12 that the voltage across the load of the receiving dipole is a sum of two pulses, each resembling the shape of the incident field pulse. These pulses are the mirror reflections because the currents flowing into the load from different dipole arms have opposite directions. The interval between these pulses is especially pronounced at small angles θ_R, when the fields incident onto different dipole arms have substantial delays. Variation in the shape of the voltage pulse across the dipole load as a function of the angle of the current pulse incident onto the dipole is similar to variation in the shape of the field pulse of the radiating dipole as a function of the observation angle. The field pattern of the receiving dipole (which is determined as the dependence of the voltage at the load on angular coordinates) demonstrates similar behavior: As the

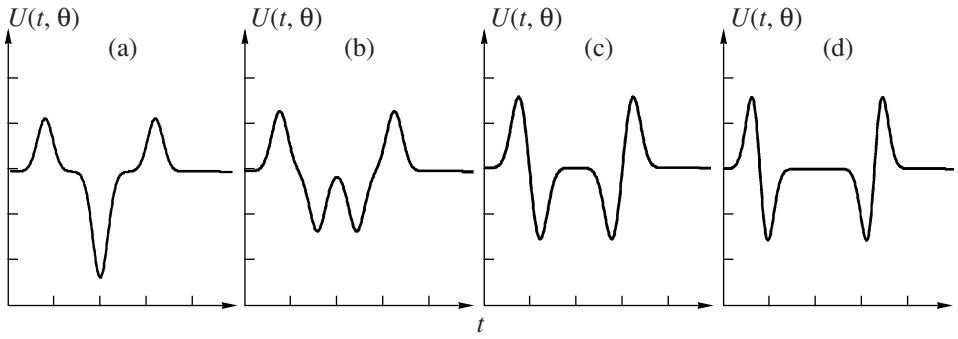

Fig. 12. Shape of the voltage across the load of the receiving antenna for θ = (a) 90°, (b) 70°, (c) 50°, and (d) 5°.

incident field pulse travels along the receiving dipole, this pattern moves in space, i.e., it becomes time-dependent. As a result, in calculations, it is necessary to use the energy pattern of the receiving dipole. This pattern is obtained via averaging of the power received from each angular direction during the time required for the pulse to travel along the dipole aperture. The energy pattern describes the distribution of the energy-density flux received by the dipole from space:

$$W_R(\theta, \varphi) = \frac{1}{Z_L}\int_{-\infty}^{+\infty} U_\Sigma^2(\theta, \varphi, t)dt,$$

The normalized energy pattern is

$$W_{RN}(\theta, \varphi) = \frac{W_R(\theta\varphi)}{W_{R\max}}.$$

where

$$W_{R\max} = \frac{1}{Z_L}\left[\int_{-\infty}^{+\infty} U_\Sigma^2(\theta, \varphi, t)dt\right]_{\max},$$

Figure 13 presents a family of 1D (φ = const) energy patterns for the above example for $L_R/c\tau = 1$, 3, and 10. If $L_R/c\tau$ is close to unity, the energy pattern coincides with the pattern of a half-wave dipole. As ratio $L_R/c\tau$ increases, the pattern shape changes: It splits into two beams, each having lesser width.

Directivity factor D_R of the receiving antenna is defined as the ratio of density $W_{R\max}$ of the energy flux received by the antenna in the direction of the pattern maximum and density W_{R0} of the energy flux received by an equivalent isotropic antenna at the same energy-flux density received from space:

$$D_R = W_{R\max}/W_{R0}.$$

The total energy of the field incident onto the antenna through a sphere with radius R is

$$W = \frac{R^2}{Z_L}\int_0^{2\pi}\int_0^{\pi}\int_{-\infty}^{+\infty} U_\Sigma^2(\theta, \varphi, t)\sin\theta d\theta d\varphi dt.$$

Dividing this energy by the surface area of the sphere surrounding the antenna, we obtain the density of the energy flux received by the equivalent isotropic antenna:

$$W_{R0} = \frac{W}{4\pi R^2}$$
$$= \frac{1}{4\pi Z_L}\int_0^{2\pi}\int_0^{\pi}\int_{-\infty}^{+\infty} U_\Sigma^2(\theta, \varphi, t)\sin\theta d\theta d\varphi dt.$$

The obtained expressions can be used to determine the energy directivity factor of a receiving antenna:

$$D_R = 4\pi\frac{\left[\int_{-\infty}^{+\infty} U_\Sigma^2(\theta, \varphi, t)dt\right]_{\max}}{\int_0^{2\pi}\int_0^{\pi}\int_{-\infty}^{+\infty} U_\Sigma^2(\theta, \varphi, t)\sin\theta d\theta d\varphi dt}.$$

5. FEATURES OF DETECTION OF UWB SIGNALS

Ultrawideband signals allow obtainment of the target pattern and recognition of the target type; in the case of very high resolution, such signals can be used to obtain the target's radio image. However, the recognition procedure is preceded by the detection procedure.

In Sections 2 and 4, we considered variations in the shape of a UWB signal during radiation and reception in the case when the inequality $c\tau \gg L$ is fulfilled.

Additional variations in the signal shape occur when the signal is reflected from the target. Spectrum $U_{\text{inc}}(\omega)$ of the signal incident onto the target and spectrum

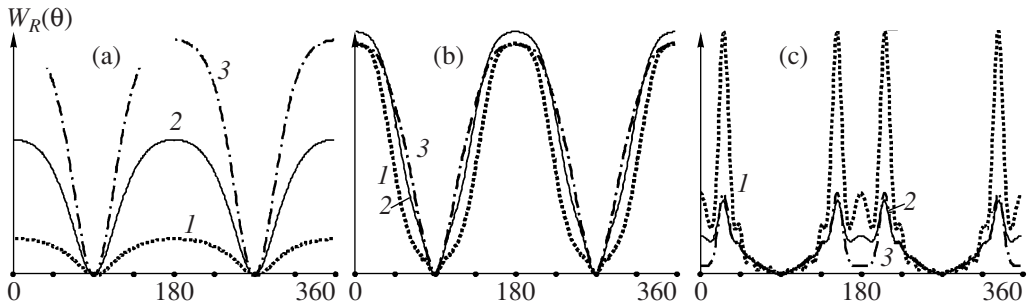

Fig. 13. Energy patterns of the receiving antenna for $L_R/c\tau$ = (a) 1, (b) 3, and (c) 10 and θ_T = (curve *1*) 30°, (curve *2*) 60°, and (curve *3*) 90°.

$U_{ri}(\omega)$ of the signal from the *i*th local scattering center are related as follows:

$$U_{ri}(\omega) = U_{\text{inc}}(\omega)K_i(\omega),$$

where $K_i(\omega)$ is the complex frequency characteristic of the *i*th local scattering center.

In a relatively narrow frequency band, we can assume that the frequency response of a local scattering center is uniform and the center's phase response is linear. Therefore, in the case of reflection of a narrowband signal from a local scattering center, the signal spectrum and shape do not change:

$$U_{\text{inc}}(\omega) \approx U_{ri}(\omega).$$

Differences arise only in the changed amplitude and initial phase of the reflected signal. This fact allows processing of a narrowband signal with the use of a correlator with a reference signal or a matched filter.

However, in a wide frequency band, nonuniformity of the frequency response and nonlinearity of the phase response of a local scattering center must be taken into account. These factors cause changes in the spectrum of a UWB signal during its reflection from the target: $U_{\text{inc}}(\omega) \neq U_{ri}(\omega)$. Changes in the signal spectrum cause an additional change in the signal shape (see Fig. 2c). Therefore, under the conditions of inequality $c\tau \gg L$, we obtain the problem of detection of a signal whose shape is unknown.

Theoretical validation of an optimum algorithm for detection of a signal in the form of a packet of identical pulses with an unknown shape and an unknown repetition rate in the presence of white Gaussian noise was performed by V.S. Chernyak [24]. The detection algorithm was synthesized with the use of a priori information on the repetition period of sounding pulses, T_p.

The target is illuminated with pulses having duration τ. The pulses' repetition rate is such that, within a relatively small interval, we can assume that the target is immobile and we can represent signal $u_\text{s}(t)$ as a packet consisting of M identical pulses (Fig. 14):

$$u_\text{s}(t) = \sum_{k=0}^{M-1} u_\text{r}(t - kT_\text{p}),$$

where $u_\text{r}(t)$ is the signal (a pulse with an unknown shape, duration T, and energy E_s) reflected from the target.

Individual pulses of a packet do not overlap; i.e.,

$$\int_{-\infty}^{\infty} u_\text{r}(t - kT_\text{p})u_\text{r}(t - mT_\text{p})dt = \begin{cases} E_\text{s}, & k = m, \\ 0, & k \neq m. \end{cases} \quad (8)$$

The noise is assumed to be Gaussian and to have zero mean value. The input signal is the mean value of the sum of the signal and noise.

For the known signal, the logarithm of the ratio of likelihood functionals has the form (see, e.g., [25])

$$\ln\Lambda = \ln\frac{W_{\text{s/n}}[u(t)]}{W_\text{n}[u(t)]} = \sum_{k=0}^{M-1}\int_{-\infty}^{\infty} u(t)u_\text{r}(t - kT_\text{p})dt - \frac{1}{2}\sum_{k=0}^{M-1}\sum_{l=0}^{M-1}\int_{-\infty}^{\infty} u_\text{r}(t - kT_\text{p})u_\text{r}(t - lT_\text{p})dt. \quad (9)$$

Here, $u(t)$ is the received realization of the sum of the signal and noise (or only noise) with duration $T_0 > (M-1)T_\text{p} + T$.

Taking into account (8), we can simplify (9) as

$$\ln\Lambda = \sum_{k=0}^{M-1}\int_{-\infty}^{\infty} u(t)u_\text{r}(t - kT_\text{p})dt - \frac{1}{2}\sum_{k=0}^{M-1}\int_{-\infty}^{\infty} u_\text{r}^2(t - kT_\text{p})dt. \quad (10)$$

Since signal $u_\text{r}(t)$ is unknown (but not random), we apply the adaptive approach. The essence of this approach lies in application of an algorithm that is optimal for known signal parameters in the situation when,

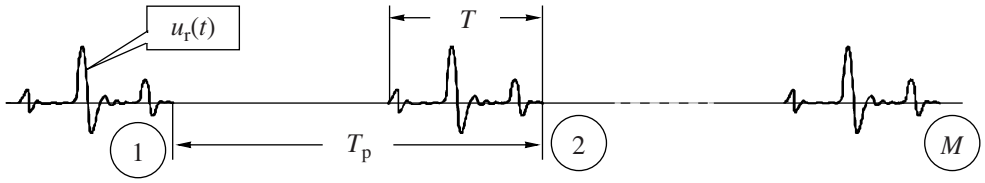

Fig. 14. Example of a periodic signal with an unknown shape.

in this algorithm, unknown parameters are replaced with their maximum-likelihood estimates [26]. In this case, we should estimate the whole signal as a function of time rather than individual signal parameters [27].

In order to obtain the estimate, we consider the logarithm of the likelihood functional [28]

$$\mathcal{R}_1 = -\frac{1}{2}\int_{-\infty}^{\infty}\left[u(t) - \sum_{k=0}^{M-1} u_r(t - kT_p)\right]^2 dt.$$

The maximum of functional $\mathcal{R}_1$ considered as a function of $\sum_{k=0}^{M-1} u_r(t - kT_p)$ corresponds to the minimum of the expression in square brackets. Since the duration of received realization $u(t)$ of the sum of the signal and noise comprises all arriving signals, the minimum of the expression in square brackets is attained under the condition that, within each time interval containing the signal, this signal is equal to the received realization:

$$\hat{u}_r(t - kT_p) = u(t) \quad \text{for} \quad t \in (kT_p, kT_p + T). \qquad (11)$$

Let us perform the change of variables in (11): $t_1 = t - kT_p$. Then, we obtain

$$\hat{u}_r(t_1) = u(t_1 + kT_p) \quad \text{for} \quad t_1 \in (0, T).$$

Estimates of the same function $u_r(t_1)$ that are obtained within time intervals spaced by repetition period T_p are statistically independent because Gaussian noise within these intervals is independent. Hence, for $t_1 \in (0, T)$, maximum-likelihood estimate $\hat{u}_r = (t_1)$ refined with the use of M measurements has the form

$$\overline{\hat{u}_r(t_1)} = \frac{1}{M}\sum_{k=0}^{M-1} ut_1 + kT_p \text{ for } t_1 \in (0, T). \qquad (12)$$

After the change of variables $t_1 = t - kT_p$ in (10), we obtain

$$\ln\Lambda = \sum_{k=0}^{M-1}\int_0^T u(t_1 + kT_p)u_r(t_1)dt_1 - \frac{1}{2}\sum_{k=0}^{M-1}\int_0^T u_r^2(t_1)dt_1. \qquad (13)$$

Replacing $u_r(t_1)$ with obtained estimate $\overline{\hat{u}_r(t_1)}$ from (12), omitting the subscript of t_1 and inessential factor $1/M$, and performing simple transformations, we obtain from (13) an adaptive detection algorithm that is optimal according to the criterion of the generalized likelihood ratio:

$$\mathcal{R} = U_{out} = \int_0^T\left[\sum_{k=1}^{M-1} u(t + kT_p)\right]^2 dt \underset{<}{>} U_{threshold}, \qquad (14)$$

where $U_{threshold}$ is the detection threshold.

Thus, the optimum algorithm is reduced to summation of the segments (with duration T each) of the received realization within those time intervals where signals are expected, calculation of the energy of this sum, and comparison of the obtained energy with a threshold whose value is determined by the specified probability of a false alarm. This is the well-known energy detector, which uses not only the energy of each pulse from the packet but also the energy of correlation coupling between these pulses. The block diagram of such a detector is shown in Fig. 15.

In the case of a sufficiently rapid motion of the target relative to the radar, pulses $u_s(t)$ of the packet become different. In this situation, at least two adjacent pulses may be assumed identical. Therefore, let us consider the practically important case of processing two signals ($M = 2$). The block diagram of the detector corresponding to this case is shown in Fig. 16. At $M = 2$, optimum algorithm (14) can be represented in the form

$$\mathcal{R} = U_{out} = \int_0^T u^2(t)dt + \int_0^T u^2(t + T_p)dt + 2\int_0^T u(t)u(t + T_p)dt \underset{<}{>} U_{threshold}. \qquad (15)$$

The first and second integrals in (15) describe an algorithm for calculation of the energy of signals received within two adjacent periods, and the third integral determines an algorithm of mutual correlation processing of these signals.

It is seen from (15) that the analyzed detector can be represented in the form of two suboptimal detectors (Fig. 17). The first detector is the detector using the sum of the energies of realization segments corresponding

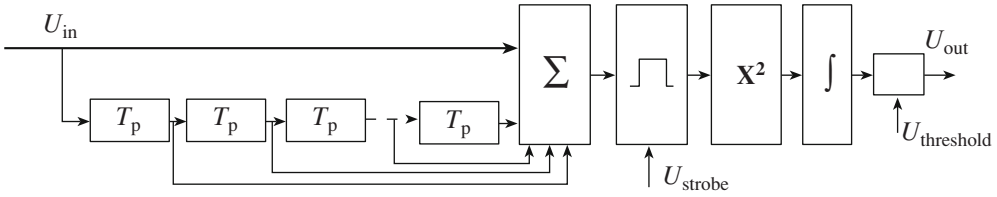

Fig. 15. Optimal detector of a packet of identical pulses with an unknown shape.

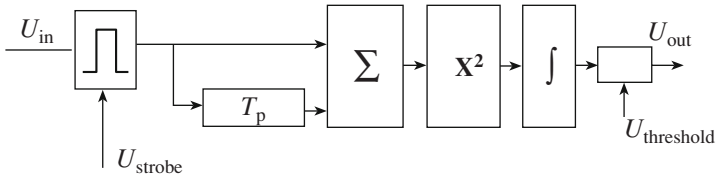

Fig. 16. Optimal detector for $M = 2$.

to expected signals in the first and second repetition periods. The second detector, which is referred to as an interperiod correlation detector (IPCD), was proposed earlier [29].[5] Block diagrams in Figs. 16 and 17 allow us to reveal the features of an optimal detector:

(i) Since the noises arriving from adjacent repetition periods are independent, the integrator input is fed with either the squared sum of the independent segments of normal processes (Fig. 16) or the sum of two squared segments and the product of these segments (Fig. 17). In both cases, the probability distribution at the integrator input is substantially different from a normal distribution.

(ii) As the integration time increases, the probability distribution of the process at the integrator output approaches a normal distribution. This time depends on the duration $T = n\tau$ of the signal reflected from the target rather than duration τ of the radiated signal. Hence, the target's radial length, $L = nc\tau/2$, determines the integration time; the degree of normalization of the distribution of the process at the integrator output; and, as a result, the level of the detector threshold.

Let us compare the efficiencies of optimal detector (15) and suboptimal detectors.

Figure 18 presents detection characteristics, which were obtained via calculation with MATLAB, for the optimum algorithm (curve *2*), the IPCD algorithm (curve *3*), and the sum of energy detectors (curve *4*). For comparison, the detection characteristic (curve *1*) of a classical detector of an exactly known (deterministic) signal is given also. The probability of a false alarm is $P_{fa} = 10^{-3}$. The characteristics were obtained for a target whose radial length comprises 16 resolution elements. With such accumulation in the process of integration, the output characteristics of both optimal and suboptimal detectors can be approximately considered Gaussian quantities. For $M = 2$, curve *3* merges with curve *4*. As seen from the figures, the absence of information on the signal shape causes substantial loss. Theis loss is due to the absence of a noise-free reference of the detected signal in the receiver.

It follows from curves in Fig. 18 that, for the considered (typical) case, suboptimal detectors have an efficiency only slightly lower than the optimum detector. Therefore, in some situations, a sufficiently simple IPCD algorithm can find practical application.

Block diagrams in Figs. 15 and 16 are optimal for detection of an immobile target (when all received pulses have identical shapes) with known radial length (when duration T of the received signal is known). This case can be used for estimation of the efficiency loss in the case of a moving target with unknown length. (Similarly, the classical theory allows estimation of the lowering of the detection efficiency in the case of unknown signal parameters by means of comparison with the detection characteristics of a deterministic signal with completely known parameters.) In real situations, when the signal velocity and length are a priori unknown, a multichannel system is required. A sequential (in time) search is possible along the signal delay (in determination of the target range); however, a parallel search is required along the duration of the integration interval (the target's radial length).

6. DETERMINING THE TARGET RCS WITH THE USE OF UWB SIGNALS

If the target is illuminated by a narrowband signal, when the target's radial length is such that $c\tau \gg L$ and reflections from different local scattering centers of the target overlap in space and form the sum signal at the reception point, the RCS of a target located in the

[5] In [29], a quasi-optimal interperiod correlation detector was erroneously called an optimal interperiod correlation detector.

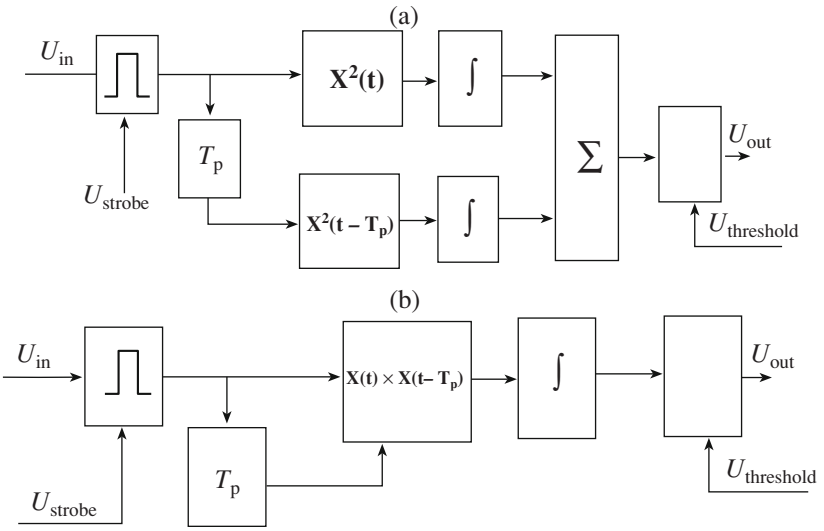

Fig. 17. Suboptimal detectors for $M = 2$: (a) an energy-sum detector and (b) an interperiod correlation detector.

antenna's far zone is determined from the well-known expression

$$\sigma = 4\pi R^2 \frac{E_2^2}{E_1^2}, \tag{16}$$

where R is the target range, E_1 is the amplitude of the field intensity of the sounding signal at the target point, and E_2 is the amplitude of the field intensity of the signal scattered by the target at the reception point.

If the target is illuminated by a UWB signal ($c\tau \ll L$), when the distances between the target's specular points are $\Delta l > c\tau$, the signals reflected from the target are separated in space. The signal at the reception point is a sequence of pulses that have different amplitudes and polarities that are shifted relative to each other by different time intervals (see the example in Fig. 2c). As a result, amplitude E_2 at the reception point becomes indeterminate [30–32].

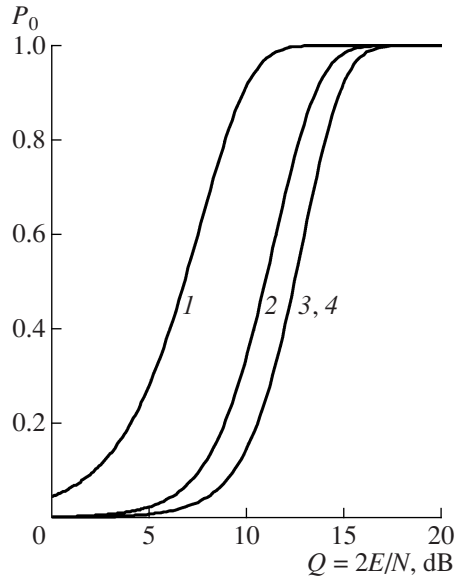

Fig. 18. Detection characteristics of the optimal and suboptimal algorithms.

In this case, the concept of a generalized RCS [33] should be used:

$$\sigma = 4\pi R^2 \frac{W_2}{W_1}, \tag{17}$$

where $W_1 = \int_{\tau_1} \Pi_1(t)dt$ is the energy of the radar's sounding signal at the target point, $W_2 = \int_{\tau_2} \Pi_2(t)dt$ is the energy of the signal scattered by the target at the reception point, $\Pi_1(t)$ is the Poynting vector (the energy-flux density) of the sounding signal acting during time τ_1 at the target point, and $\Pi_2(t)$ is the Poynting vector (the energy-flux density) of the scattered signal acting during time τ_2 at the reception point.

In order to estimate the applicability of formula (17), we compare the RCSs obtained in the cases of illumination of the target with a narrowband signal and a UWB signal. Let the target be the simplest clustered secondary radiator consisting of two radiators (a dumbbell). We assume that the reflectors do not influence on each other.

In the case of a narrowband signal ($c\tau \gg L$), the result is well known [34]. The field pulse illuminating the target has the HF carrier $e_1(t) = E_1\cos\omega t$. Let us designate the distances from the radiators to the radar as $r_{1,2}$ ($r_1 - r_2 = \Delta l \ll c\tau$) and the times of arrival of reflected fields at the reception point as $t_{1,2} = 2r_{1,2}/c$.

The field scattered by a secondary radiator at the reception point is calculated from the formula

$$e_2(t) = E_{2(1)}\cos\omega(t - t_1) + E_{2(2)}\cos\omega(t - t_2) = E_2\cos(\omega t - \varphi),$$

where the subscript in parentheses denotes the reflector number and $\varphi = \omega(t_1 - t_2) = \frac{2\pi}{\lambda}2(r_1 - r_2) = 4\pi\Delta l/\lambda$.

The total amplitude of field E_2 at the reception point is

$$E_2^2 = E_{2(1)}^2 + E_{2(2)}^2 + 2E_{2(1)}E_{2(2)}\cos\varphi.$$

In accordance with (16), the target RCS is

$$\sigma_{\Sigma 2} = 4\pi R^2\frac{E_2^2}{E_1^2} = \sigma_1 + \sigma_2 + 2\sqrt{\sigma_1\sigma_2}\cos\varphi.$$

If $\varphi = 0$ and $\sigma_1 = \sigma_2 = \sigma$, the RCS is maximal, $\sigma_\Sigma = 4\sigma$. Accordingly, in the case of N reflectors with equal RCSs σ and equiphase reflected fields, the RCS of a clustered radiator is $\sigma_{\Sigma N} = N^2\sigma$. In the general case, phase φ is a random quantity that takes arbitrary values ranging from 0 to 2π. In this case, the RCS of a target illuminated by a narrowband (NB) signal is determined as the mean value

$$\sigma_{\text{NB}} = \bar{\sigma}_{\Sigma N} = N\sigma. \quad (18)$$

In the case of a UWB signal ($c\tau \ll L$), the considered secondary radiator is illuminated by a field pulse with duration τ and energy-flux-density $\Pi_1(t)$. If $r_1 - r_2 = \Delta l > c\tau/2$, we have two nonoverlapping field pulses that are reflected from two reflectors and that arrive at the reception point. Generally, these pulses have different energy-flux densities $\Pi_{2(1)}(t)$ and $\Pi_{2(2)}(t)$ and different durations τ_1 and τ_2.

In this case, the RCS of each secondary radiator is determined from formula (17):

$$\sigma_{1,2} = 4\pi R^2\frac{W_{2(1),2(2)}}{W_1},$$

where $W_1 = \int_\tau \Pi_1(t)dt$ is the energy of the radar sounding signal at the target point and $W_{2(1)} = \int_{\tau_1} W_{2(1)}(t)dt$ and $W_{2(2)} = \int_{\tau_2} \Pi_{2(2)}(t)dt$ are the energies of the signals that arrive at the reception point from the first reflector at time t_1 and from the second reflector at time t_2.

When signals from each reflector are received separately, the RCS of the entire radiator is determined by the reflector that generates the highest amplitude of the signal in the radar receiver. The energy arriving at the reception point from the smaller reflector is not used. This circumstance can be treated as a loss. If the number of radiators increases, this loss likewise increases.

In order to maximize the RCS of a target illuminated by a UWB signal, it is necessary to use the energy of the signal at the output of the optimal processing system (see Section 6).

Let us estimate the RCS of the considered secondary radiator consisting of two identical reflectors ($M = 2$) in the case of optimal processing of two pulses traveling one after another with an interval equal to the repetition period. After substituting two reflected pulses in each period (where the subscript denotes the reflector number) into formula (15), we obtain an expression that is proportional to the energy of the received signal at the output of the processing system:

$$U_{\text{out}} = \int_0^T u_1^2(t)dt + \int_0^T u_2^2(t)dt + \int_0^T u_1^2(t + T_\text{p})dt + \int_0^T u_2^2(t + T_\text{p})dt + 2\int_0^T u_1(t)u_2(t)dt + 2\int_0^T u_1(t + T_\text{p})u_2(t + T_\text{p})dt + 2\int_0^T u_1(t)u_2(t + T_\text{p})dt + 2\int_0^T u_2(t)u_1(t + T_\text{p})dt + 2\int_0^T u_1(t)u_1(t + T_\text{p})dt + 2\int_0^T u_2(t)u_2(t + T_\text{p})dt.$$

The first four integrals determine the energy of the first and second signal pulses in the first and second repetition periods. The next six integrals determine the mutual energy of various pulse pairs. The first four of these six integrals describe the mutual energy of the pulses nonoverlapping in time and, therefore, take values of zero. The remaining two integrals determine the mutual energy of two overlapping (after a delay by T_n) pulse pairs. Thus, the total energy of the received signal, which determines the output voltage of the processing system, is

$$W_2 = \int_0^T u_1^2(t)dt + \int_0^T u_2^2(t)dt + \int_0^T u_1^2(t + T_\text{p})dt + \int_0^T u_2^2(t + T_\text{p})dt + 2\int_0^T u_1(t)u_1(t + T_\text{p})dt + 2\int_0^T u_2(t)u_2(t + T_\text{p})dt = W_{2(1,1)} + W_{2(1,2)} + W_{2(2,1)} + W_{2(2,2)} + 2W_{2(1,1-2,1)} + 2W_{2(1,2-2,2)},$$

where the first and second subscripts in parentheses are the period number and the reflector number, respectively.

If the energy of the radar's sounding signal at the target point is W_1, then, after substituting the obtained energies into (17), we have

$$\sigma_{\Sigma 2} = 4\pi R^2 \frac{W_{2(1,1)} + W_{2(1,2)} + W_{2(2,1)} + W_{2(2,2)} + 2W_{2(1,1-2,1)} + 2W_{2(1,2-2,1)}}{W_1}$$
$$= \sigma_1 + \sigma_1 + \sigma_2 + \sigma_2 + 2\sigma_{1-2} + 2\sigma_{2-1}.$$

If $\sigma_1 = \sigma_2 = \sigma_{1-2} = \sigma_{2-1} = \sigma$, we obtain $\sigma_{\Sigma 2} = 8\sigma$. This value of the RCS is obtained with consideration for the energy reflected from the target within two sounding periods. For one sounding period, the ratio of the energy at the reception point to the energy at the target point gives the following RCS: $\sigma_{\Sigma 2} = 4\sigma$. Accordingly, for N secondary radiators with equal RCSs σ, the total RCS of a clustered radiator is

$$\sigma_{\Sigma N} = N^2\sigma. \quad (19)$$

Comparing RCSs (18) and (19), which correspond to illumination of the same target consisting of N reflectors by NB and UWB signals, respectively, we see that the inequality $\sigma_{\Sigma N} \geq \bar{\sigma}_{\Sigma N}$ is satisfied. Hence, $\sigma_{\mathrm{UWB}} \geq \sigma_{\mathrm{NB}}$.

In the general case of arbitrary RCSs of individual reflectors of the target, target RCS σ_Σ depends on the amplitude of the output signal of the optimal processing system, which is proportional to the signal energy. The output of the optimal processing system is the reception point used in formulas (16) and (17). Since the RCS is determined from the energy of the signal reflected from the target, below, σ_Σ is referred to as the energy RCS.

7. RANGE EQUATION: FEATURES OF THE APPLICATION OF UWB RADARS

The traditional range equation of a narrowband radar usually involves parameters related to the harmonic (or quasi-harmonic) shape of the used signal. The amplitude of this signal determines the peak and mean radar powers and the RCS of the target. The radiation and reception patterns, which determine the directivity factors of receiving and transmitting antennas, are the results of the spatial interference of harmonic oscillations radiated by individual antenna elements.

In a UWB radar, the shape of the signal varies in the process of radar observation. Therefore, range R of a UWB radar is determined through energy parameters:

$$R = \sqrt[4]{\frac{WD_T\sigma_\Sigma S}{(4\pi)^2 \rho q N_0}}, \quad (20)$$

where $W = \int_\tau p(t)dt$ is the energy of the radiated signal, $p(t)$ is the radiated power as a function of time, D_T is the energy directivity factor of the transmitting antenna, D_R is the energy directivity factor of the receiving antenna, $S = \frac{D_R(c\tau)^2}{4\pi}$ is the effective (energy) area of the receiving antenna, σ_Σ is the energy RCS of the target, ρ is the loss in all systems of the radar, q is the threshold value of the energy signal-to-noise ratio, and N_0 is the spectral density of the noise power.

Energy range equation (20) is a generalized relationship because this equation can be used for calculation of the radar parameters at any relationships between signal duration $c\tau$ and antenna (and/or target) dimension L. However, if $L \gg c\tau$, only range equation (20) can be used for calculations.

Let us consider factors limiting the range of a UWB radar. A high information efficiency of UWB radars is attained with the use of nanosecond and picosecond pulses. In the case of radiation of simple short pulses similar to those shown in Fig. 2, the energy required for target detection can be obtained only via an increase in peak power P_{peak}. Let us estimate the value of this power via a particular example. To simplify calculations, we assume that $W \approx P_{\mathrm{peak}}\tau$ and we determine P_{peak} in terms of the parameters of the range equation:

$$P_{\mathrm{peak}} = \frac{(4\pi)^2 \rho q N_0 R^4}{D_T \sigma_\Sigma S \tau}.$$

Figure 19 presents the transmitter's peak power as a function of the range of a UWB radar for different values of pulse duration τ. The radiated signal is received in the form of a Gaussian pulse with a unit amplitude and duration τ at a level of 0.5. (The shape of this signal is shown in Fig. 4, curve *2*.) For calculation, we use the following numerical values of parameters: The energy directivity factors of antennas are $D_T = D_R \approx 1000$ (a circular aperture with a diameter of about 3 m), $\sigma_\Sigma = 0.1$ m^2, the probability of correct detection is $P_D = 0.9$, and the probability of false alarm is $P_F = 10^{-6}$.

As seen from Fig. 19, application of simple UWB signals for observation of targets at large distances requires a transmitter with a peak power of several gigawatts or even several tens of gigawatts. Generators

with such power are unique devices that require the application of components with high electric strength and that negatively effect the environment owing to the emission of X-rays and direct electromagnetic radiation.

In principle, there is a traditional way of lowering of the peak power in long-range UWB radars via passage to complex coded signals with large values of the bandwidth–duration product and subsequent matched filtering. However, variations in the shape of the UWB signal during radar observation prohibit the use of this method.

In high-power UWB radars, it is possible to obtain the required performance with the use of active pulse antenna arrays and without application of gigawatt generators. In this case, it is necessary to ensure high time stability of the system for high-precision control of the array generators. Note that application of active pulse antenna arrays in UWB radars makes these radars complex and expensive systems and that the methods of manufacturing such systems are still not adequately developed.

Nevertheless, the main obstacle to the development of UWB radars with a relatively long range is not the complexity of engineering solutions.

The high information density of UWB systems requires the use of wide segments of the frequency spectrum. Therefore, UWB radars may generate interference for many other radio systems operating in the same segments of the spectrum, e.g., satellite navigation systems (GPS, GLONASS, GALILEO), satellite search and emergency systems, and air-traffic-control systems. Therefore, the electromagnetic compatibility of UWB radars with other radio systems is one of the main problems determining the prospects of development of such systems.

Recently, this problem was solved for short-range UWB radars. In 2002, the first (in the history of radio engineering) normative document was issued that allowed simultaneous operation of UWB and narrowband radio systems in the same frequency band. This document is the First Report and Order of the US Federal Communications Commission (FCC), which was issued in April, 2002 and was supplemented in 2003 and 2004 [3, 4]. This document is the result of revision of the US Code of Federal Regulations [35] as applied to UWB systems. This document formulates limitations on the radiation levels of UWB systems in different frequency bands in the form of the so-called masks. (An example of such a mask is presented in Fig. 20.) If these limitations are fulfilled, UWB systems can be used without licensing. Today, this document is used as a reference in many countries [36].

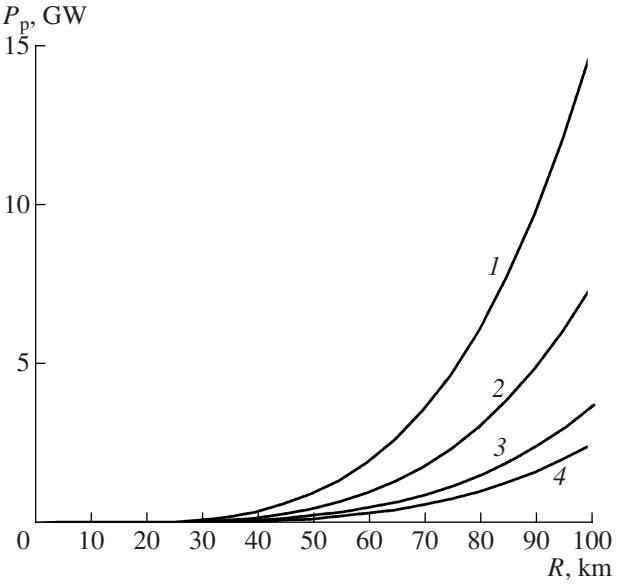

Fig. 19. Dependence of the pulsed power of a UWB radar on the detection range for τ = (*1*) 0.5, (*2*) 1.0, (*3*) 2.0, and (*4*) 3.0 ns

For long-range UWB radars, for example space UWB radars, the electromagnetic compatibility with other radio systems operating in the same segments of the spectrum are very questionable. Therefore, at present, the most reliable way to apply UWB technology in radar is the development of low-power radars operating at ranges from several meters to several tens of meters in air and in various media (for example, ground-penetrating radars). Such radars are widely used in various fields and, as a consequence, are promising commercial products.

8. FEATURES OF THE DESIGN OF SHORT-RANGE UWB RADARS: PRACTICAL APPLICATIONS

Features of calculating the parameters of UWB radars, which were discussed in preceding sections, are combined with the features of the design and application of such devices. Let us consider these features in application to a short-range radar whose outline block diagram is shown in Fig. 21.

For radiation of such short pulses, two versions of transmitters can be used.

In one version, a stable driving oscillator forms unipolar video pulses with a relative large duration (of several microseconds). In the shaper of this transmitter, the pulses are transformed into unipolar video pulses with small durations (of several nanoseconds), which perform "shock" excitation of the transmitting antenna radiating short radio pulses at its center frequency. The duration of the radiated radio pulse depends on the

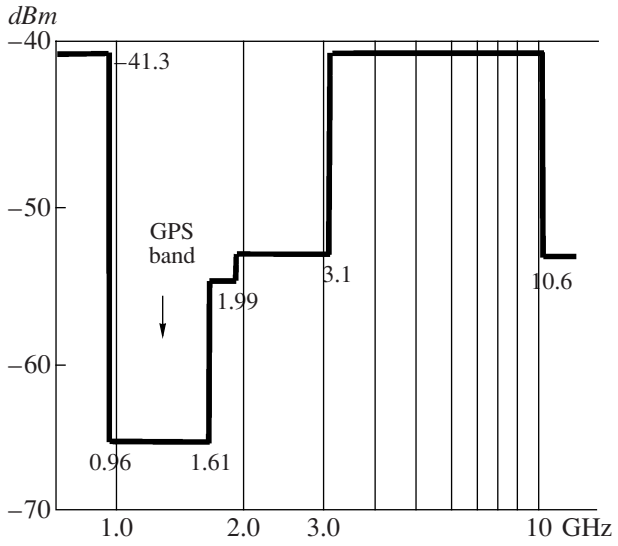

Fig. 20. Permissible radiation levels for UWB radars [3, 4].

antenna parameters. The pulses from the driving oscillator pass also through a control delay line and enter the second shaper, which forms a similar pulse enabling the receiver at the time of arrival of the reflected signal corresponding to a certain range. Radars with such transmitters are sometimes called videopulse radars. Such a transmitter has low energy characteristics because only a small part of the video-pulse spectrum falls into the antenna frequency band and is radiated into ambient space [37]. Such transmitters are used when the energy characteristics of the radar are not an issue, but a simple design solution is required.

In another version, the transmitter is designed according to a conventional coherent layout. A stable oscillator forms a continuous oscillation at the radar's carrier frequency, the shaper used in this transmitter cuts out short radio pulses from the continuous oscillation, and these radio pulses are radiated by the antenna. The same signal passes through a control delay line and enters the receiver shaper, which forms a reference signal that enables the receiver within a short time window (strobe). Varying the delay of the reference signal, it is possible to vary the distance to the observed object. All the remaining time, the receiver is disabled. This circumstance allows implementation of efficient protection from the signals reflected from the objects located beyond the working strobe.

For different types of observed targets (immobile or moving), the UWB radar operates in coherent or incoherent mode. Accordingly, an amplitude or a phase detector is used at the receiver input. In the case of application of an amplitude detector, the pulses generated at the detector output are amplified and quantized and, afterward, are fed into a microcontroller. In the case of application of a phase detector, the pulses formed at its output enter an integrating amplifier whose bandpass filter isolates the range of operating Doppler frequencies of the radar and accumulates the signal. The accumulated low-frequency (LF) signal is quantized and fed into a microcontroller. The microcontroller controls all operations of the radar in accordance with a prescribed algorithm and prepares data for subsequent processing on a computer. The computer detects the target, indicates the moving targets, and performs digital filtering of the necessary data.

In order to exclude blind zones along the range in the course of coherent processing of the signal in the receiving channel of the radar, quadrature channels (not shown in the outline block diagram in Fig. 21) are used. These channels contain phase detectors with reference signals shifted by 90°.

In some practical applications (medical investigations, the search for people in trapped in ruins and avalanches, monitoring an operator's state during hazardous work), short-range radars are used for remote and contactless determination of the physiological parameters of a person (respiratory rate and heart rate). The operating feature of such radars is the combination of a high repetition rate of the sounding pulses and low velocity of travel of the observed object. This combination allows coherent accumulation of large pulse packets (containing several hundred thousand or several million sounding pulses) within sufficiently large time intervals (of about 0.1 s) in which the observed objects are considered stationary. This circumstance allows substantial lowering of the peak and mean power of the radar transmitter, a possibility that is especially important for UWB radars operating under stringent requirements on the electromagnetic compatibility with radio equipment operating in the same frequency band.

Another feature of such radars is related to the alternating motion of the observed objects (the human thorax, the human heart), which is unusual for radar. This feature creates special conditions for the radar observation of such objects. The point is that the shape (and the spectrum) of the output signals of quadrature channels substantially depends on the ratio of amplitude ΔR of the alternating motion and wavelength λ of the radiated signal. If $\Delta R < \lambda$, the output signal of quadrature channels have shapes that are close to the real trajectory of the object. However, when the amplitude of this motion becomes comparable with the wavelength of the radiated signal, the quadrature output signals (and their spectra) acquire complex shapes that are substantially different from the actual trajectory of the moving object (Fig. 22). This case requires the application of special processing that restores the signal shape corresponding to the true object motion via calculation of the arctan-

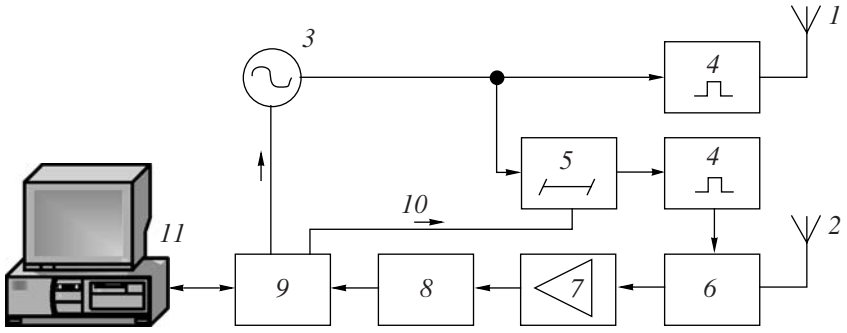

Fig. 21. Generalized block diagram of a Doppler UWB radar: (*1*) transmitting antenna, (*2*) receiving antenna, (*3*) driving oscillator, (*4*) shaper of short pulses, (*5*) delay line, (*6*) amplitude or phase detector, (*7*) integrating amplifier, (*8*) analog-to-digital converter, (*9*) microcontroller, (*10*) controller of the delay line, and (*11*) computer.

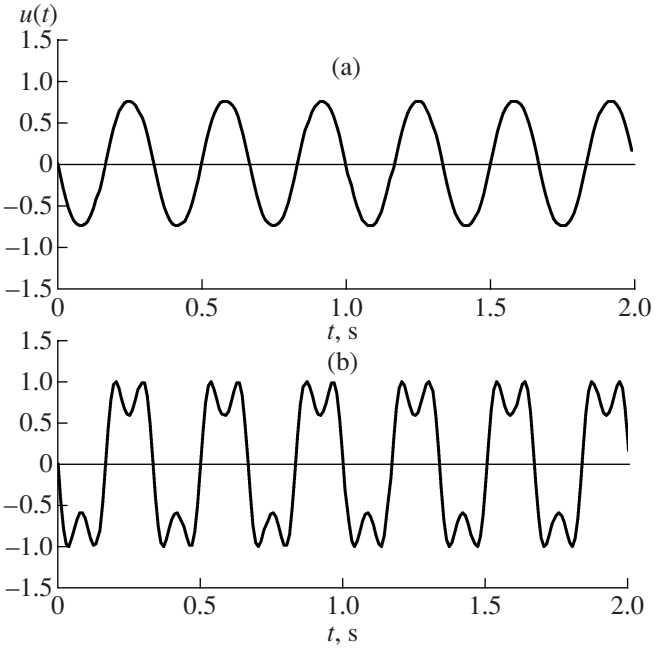

Fig. 22. Output signal of a quadrature channel in the case of alternating motion of the observed object in accordance with a harmonic law for ΔR = (a) 0.8λ and (b) 2.5λ.

gent of the ratio of the output signals in two quadrature channels.

Isolation of the signals corresponding to the respiratory rate and heart rate that are received by a UWB radar during observation of biological subjects likewise requires a nonstandard approach. The period of the thorax's motion and the period of the heart's motion are unstable over a long time interval. This violation of the periodicity of motion (or variability of the rate) is an important factor in medicine. Therefore, frequency separation of the respiratory and heart signals cannot be performed with conventional (analog or digital) filters, which, perform averaging of the signal in the course of filtering and, hence, remove the information on the signal variability. In order to isolate signals with violation of periodicity, so-called temporal filtering is used. In this filtering, one (usually, low-frequency) signal is approximated in each period by the segments of polynomials of different orders. The obtained approximation is the LF signal isolated from the sum signal. Isolation of the HF signal is performed via subtraction of the approximated LF signal from the sum signal. This filtering method retains all violations of the periodicity of motion, and the obtained data can be used for diagnostics.

Below, we present the characteristics of some short-range UWB radars developed and manufactured at the Research Center of Ultrawideband Technology of the Moscow Aviation Institute (http://www.uwbgroup.ru) and describe the operating conditions of these radars.

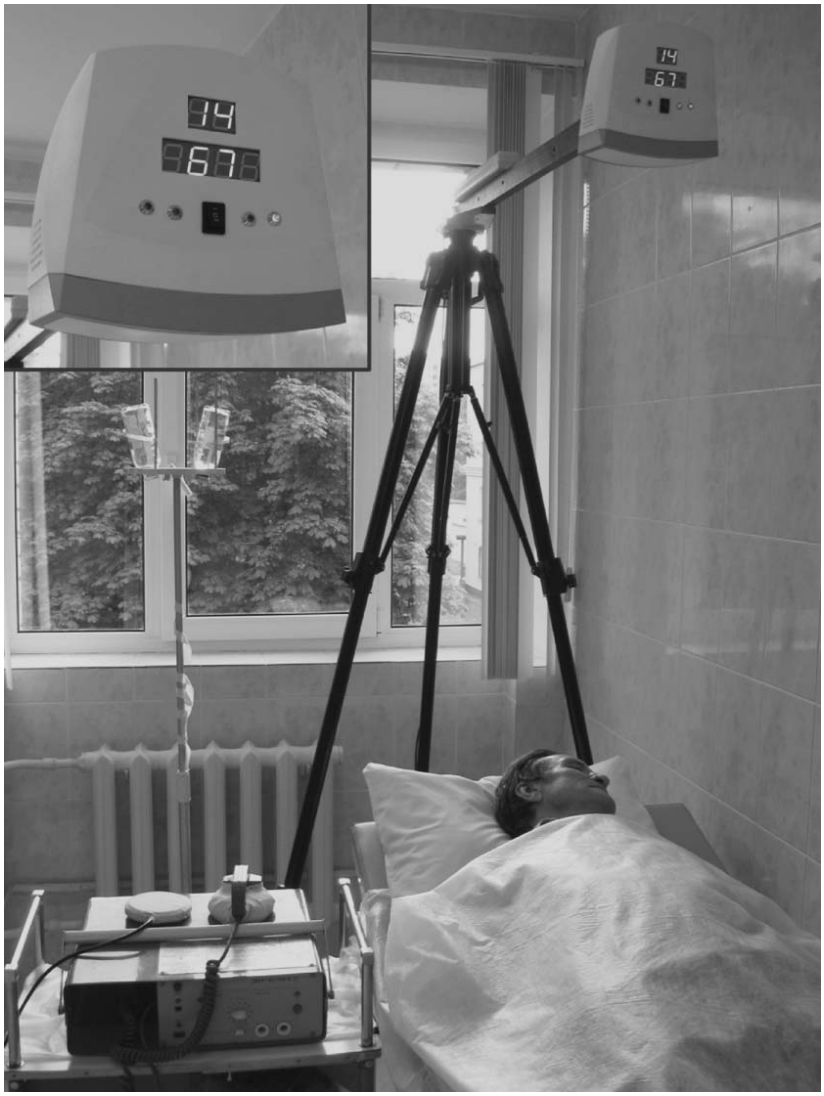

Fig. 23. Physical configuration of a medical UWB radar for remote measurements of the respiratory rate and the heart rate.

A UWB Radar for Medical Investigations

The main radar characteristics are as follows:

The range is 0.1–3.0 m.

The pulsed power is 0.4 W.

The mean power is 240 μW.

The repetition frequency is 2 MHz.

The duration of the radiated pulse is 2 ns.

The physical configuration of this radar is shown in Fig. 23, and the results of remote measurement of physiological parameters of a person with this radar are shown in Fig. 24. Figure 24a depicts the sum signal of the respiratory and heart activity that was obtained at the radar output. The level of this signal is directly proportional to the thorax's and heart's motion. Figure 24b shows the signal corresponding to only the heart motion. This signal was recorded during breath holding. In order to estimate the accuracy of measuring heart activity with the use of a UWB radar, the radar data were compared with reference electrocardiographic data, which are shown in the upper parts of Figs. 24a and 24b. The data used for comparison are variations in the systolic period between heartbeats within some time interval or the so-called variability, which is an important diagnostic factor in cardiology.

Figure 25 presents an example of the measurements of change in the variability of the heart rate that were performed simultaneously with a radar (solid curve) and an electrocardiograph (dashed curve). The correlation coefficient of these measurements, which was checked in several experiments, is no less than 0.94.

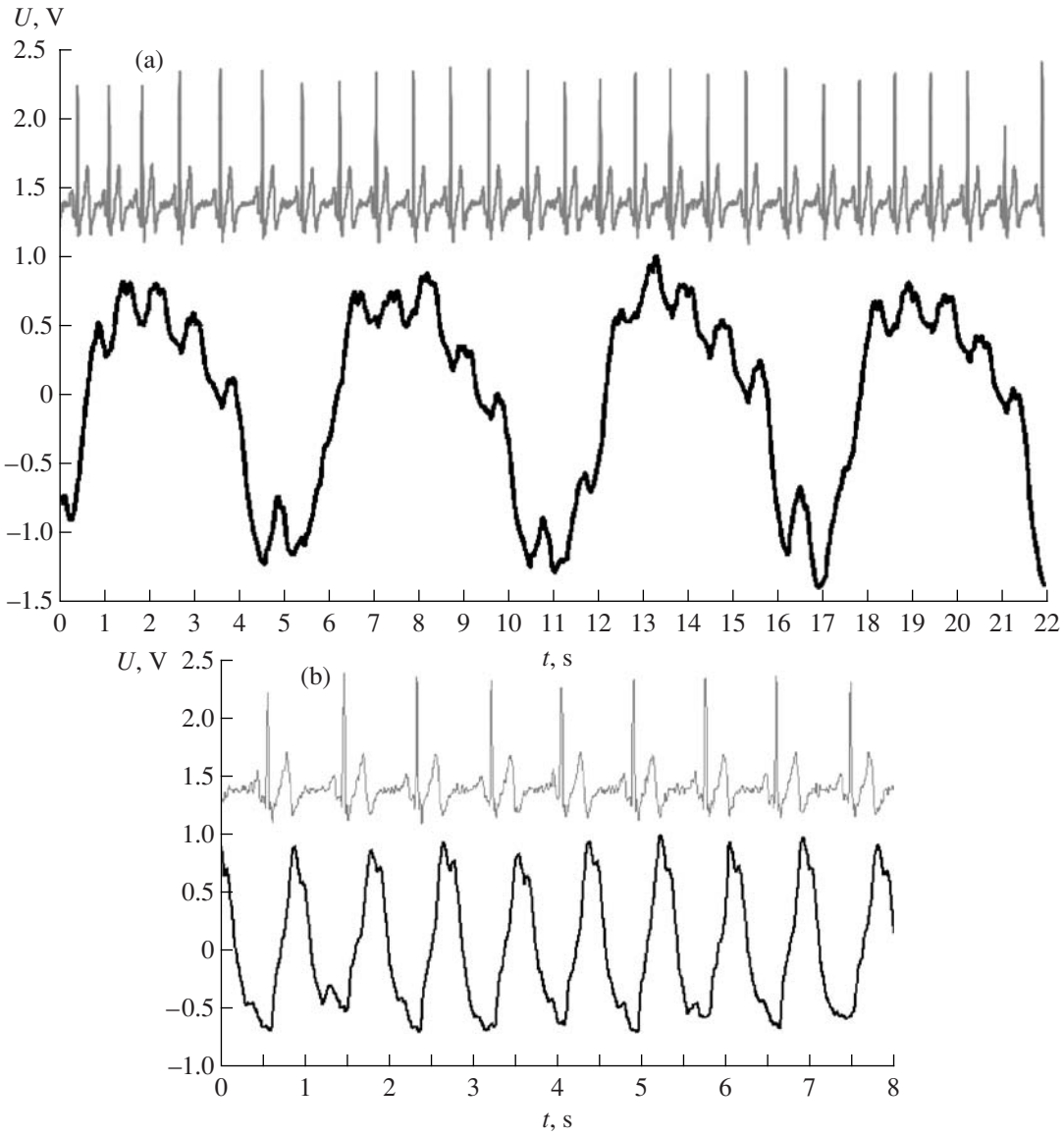

Fig. 24. Experimental results: (a) the summed curve of the respiratory rate and the heart rate and (b) the curve of only the heart rate (during breath holding).

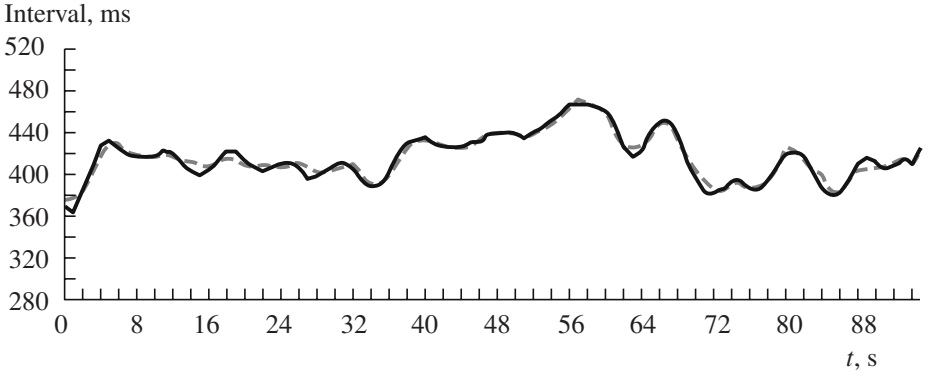

Fig. 25. Results of measuring the variability of the heart rate.

(a)

(b)

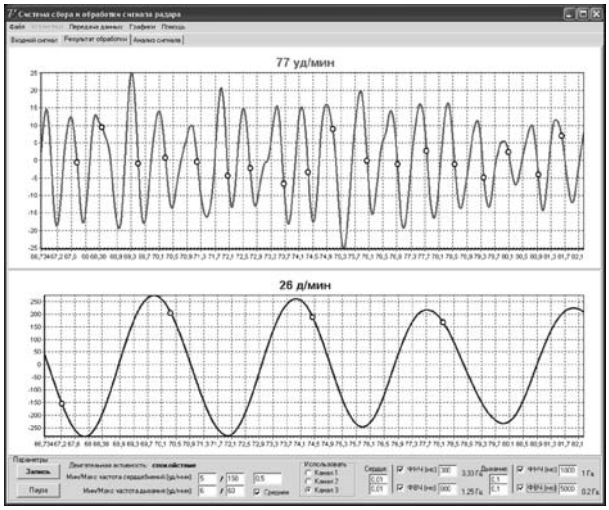

Fig. 26. (a) Ultrawideband radar for measuring the pulse and respiration at distances of up to 8 m and (b) the pulse and respiration signals at the output of this UWB radar.

A UWB Radar for Measuring the Human Physiological Parameters at Distances of up to 8 m

The physical configuration of this radar is shown in Fig. 26a, and an example of output signals is presented in Fig. 26b.

A Multifunction Medical UWB Radar

The radar consists of two sensors designed for simultaneous measuring of the pulse in blood vessels located in various parts of the body. This device can be used for measuring the speed of propagation of the pulse wave, a parameter that is important in diagnostics of heart and vascular diseases. Figure 27a shows the procedure of measuring a human's pulse wave with this radar. Figure 27b presents the signals at the outputs of radar sensors.

Simultaneously with measurement of the speed of propagation of the pulse wave, this radar measures the variability of the heart rate. In this regard, it is a convenient instrument for cardiovascular diagnostics.

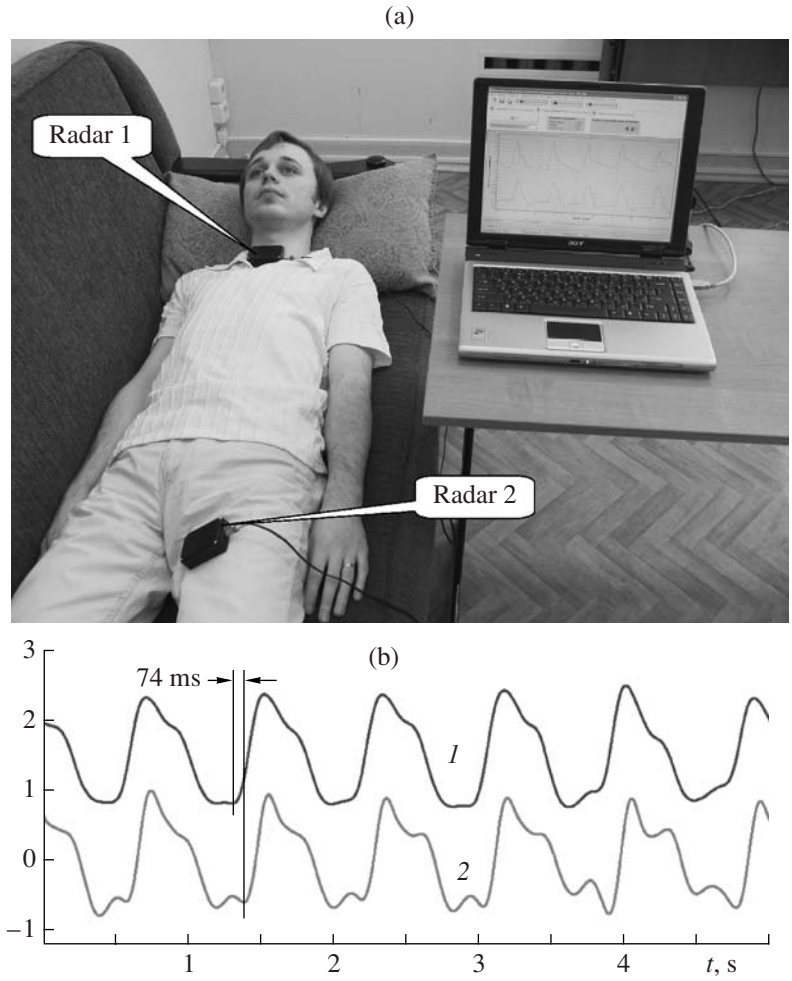

Fig. 27. (a) Physical configuration of a multifunction UWB radar for measuring the speed of the pulse wave and the variability of the heart rate and (b) radar signals from the sensors placed on (*1*) the carotid artery and (*2*) the radial artery.

Fig. 28. A Measuring UWB radar at a railway yard.

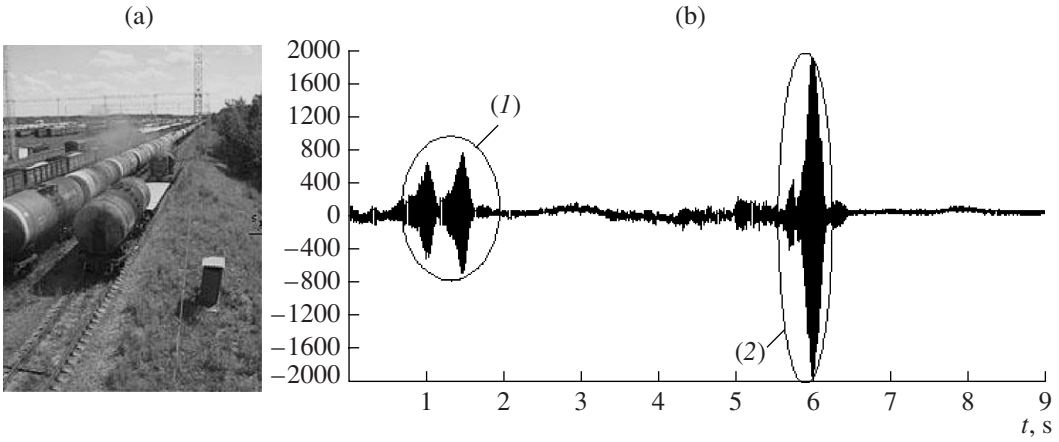

Fig. 29. Rolling stock and the results of measurement of its position: (*1*) signal from the engine and (*2*) signal from the end of a tank car.

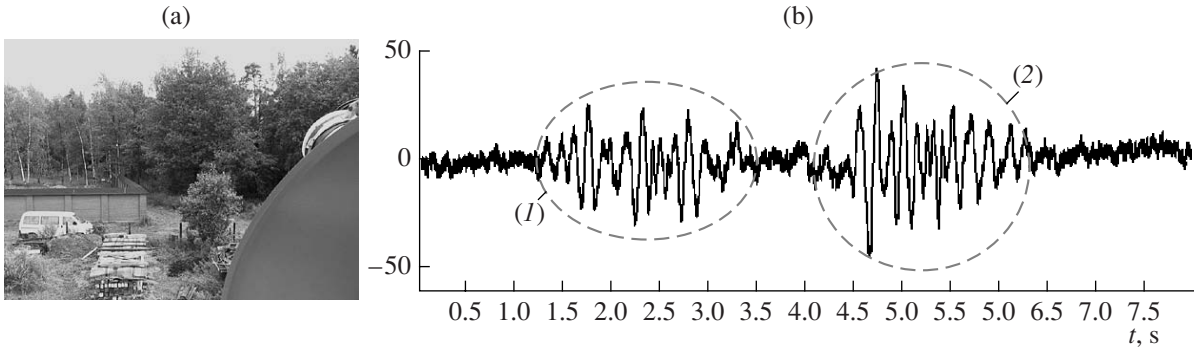

Fig. 30. (a) Forestland and (b) the results of observation of two people moving in the forest at a distance of 50 m from the forest's edge: signals from the intersections of the strobe of the UWB radar by (*1*) the first person and (*2*) the second person.

A UWB Radar for Measuring the Velocity and Location of Railway Vehicles on the Railway Lines of a Yard during Vehicle Descent from a Hump Yard

The main characteristics of this radar are as follows:

The range is 300 m.

The monitored velocity of vehicles is 10.0–0.2 m/s.

The pulsed power is 10W.

The mean power is 8.4 mW.

The range resolution is 41 cm.

The shift of the range strobe is 3.75 cm.

Figure 28 shows the position of this radar on the lighting tower of a yard, and Figs. 29a and 29b show a train moving along the yard lines and the radar signals (curves *1*, *2*) reflected from this train. The output signals of several radars placed on the yard towers are transmitted over wireless links to a control center. After processing, this information is used to form the trains.

UWB Radar for Detection of People in Bushes or a Forest

Figure 30 shows the site of the experiment and the signals from two people moving in a forest at a distance of 50 m from the edge.

A UWB Radar for Observation of Moving and Motionless Persons Located behind Barriers in the Form of Walls Made of Various Materials

Figure 31a shows the output signals of a radar placed at a distance of about 1 m from a brick wall with a thickness of 50 cm. During the experiment, a man situated behind the wall (*1*) began to move in the premises; (*2*) then stood still; and, after a time, (*3*) resumed his motion. In the first and third segments of the curve in Fig. 31a, we see the high-amplitude signal corresponding to the man's motion. In the second segment, when the man is motionless, we see the signal caused only by the motion of his thorax (the periodic signal in

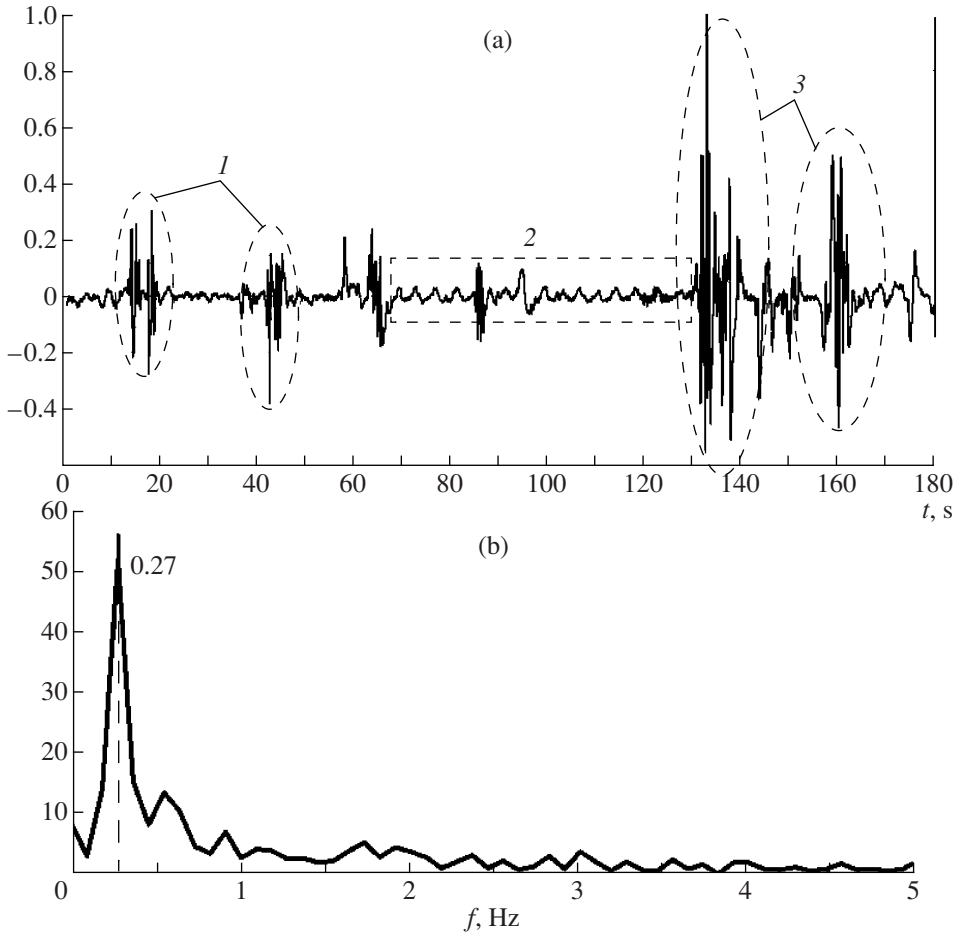

Fig. 31. Remote detection of people located behind barriers: (a) radar signals (*1*, *3*) from a moving man and (*2*) from a motionless man located behind a brick wall at a distance of 50 cm from the wall and (b) a spectrum of signal *2*.

the rectangular frame). Figure 31b presents the amplitude spectrum of the framed signal fragment in Fig. 31a. The spectrum maximum corresponds to the man's respiratory rate.

CONCLUSIONS

I am well aware of the difficulty of my attempt to present here some generalization of the operating and design features of UWB radars. One consolation may be the remark of the originator of this line of research, Dr. H Harmuth, which he made in 1981, and which is valid today [2]. He wrote that relative frequency bandwidth η can take any value in the interval $0 < \eta < 1$. Our modern technology is based on the theory developed for the limiting case of $\eta \longrightarrow 0$. Both the theory and the technology applicable for the entire range $0 < \eta < 1$ must be more general and more complex than the theory and technology related to only the simplest case of $\eta \longrightarrow 0$. M. Skolnik's *Radar Handbook*, which presents a brief description of the issues related to the case of $\eta \longrightarrow 0$, gives a certain insight into the problems that could be faced in the general case of $0 < \eta < 1$. Writing the *Radar Handbook* took forty years of the development of radar, including several technological revolutions. This fact indicates that many years will pass before a similar handbook will be issued for the general case.

Now, 25 years later, the insufficiency of the theoretical basis for the development of UWB technique and technology as a system and as a tool for the design of individual devices, especially antenna systems, remains an obstacle to further progress. Therefore, I hope to attract the interest of the specialists working in this field to the viewpoint presented, especially because the new potential provided by UWB radio systems for improving the quality and increasing the amount of the transmitted information attract yearly increasing funds and intellectual resources in many countries for the development of such systems.

ACKNOWLEDGMENTS

I am grateful to Lev Astanin and Viktor Chernyak (Russia), as well as James D. Taylor and Stephen

Johnson (USA), for their continued support of this study and their abundance of friendly advice.

REFERENCES

1. C. Shannon and W. Weaver, *The Mathematical Theory of Communication* (University of Illinois Press, Urbana, 1949).
2. *Introduction to Ultra-Wideband Radar Systems*, Ed. by J. D. Taylor (CRC Press, Boca Raton, 1995).
3. FCC 02-48, ET Docket 98-153, First Report and Order, April 2002.
4. FCC 04-285, ET Docket 98-153, Second Report and Order and Second Memorandum Opinion and Order, December 2004.
5. H. F. Harmuth, *Nonsinusoidal Waves for Radar and Radio Communication* (Academic, New York, 1981; Mir, Moscow, 1985).
6. L. Yu. Astanin and A. A. Kostylev, *Theory of Ultrawideband Radar Measurements* (Radio i Svyaz', Moscow, 1989) [in Russian].
7. I. Ya. Immoreev, Vopr. Spets. Radioelektron., Ser. Radiolokatsionnaya Tekhnika, No. 22, 76 (1991).
8. Ultra-Wideband Radar Technology, Ed. by J. D. Taylor (CRC Press, Boca Raton, 2000).
9. M. L. Osipov, Radiotekhnika, No. 3, 3 (1995).
10. B. V. Bunkin and V. A. Kashin, Radiotekhnika, Nos. 4–5, 128 (1995).
11. I. Ya. Immoreev, Elektromagn. Volny Elektron. Sist. **2** (1), 81 (1997).
12. I. Ya. Immoreev, Vestn. MGTU, No. 4, 25 (1998).
13. I. Immoreev, in *Ultra-Wideband Radar Technology*, Ed. by J. D. Taylor (CRC Press, Boca Raton, 2000), p. 1.
14. O. N. Linnikov, Yu. G. Sosulin, V. I. Suvorov, et al., in *Ultrawideband Signals in Radar and Acoustics: UWSRA-2006 (Proc. 2nd All-Russia Conf., Murom, Russia, July 4–7, 2006)* (Vladimir Gos. Univ., Vladimir, Russia, 2006), p. 420 [in Russian].
15. S. L. Zlobin, M. L. Osipov, and V. N. Skosyrev, Radiotekhnika, No. 12, 18 (1999).
16. I. Ya. Immoreev and A. N. Sinyavin, in *Antenny* (Radiotekhnika, Moscow, 2001), No. 1, p. 8 [in Russian].
17. N. Zaiping, IEEE Trans. Electromagn. Compat. **25**, 24 (1983).
18. P. Feynman, R. B. Leighton, and M. Sands, *The Feynman Lectures on Physics* (Addison-Wesley, Reading, Mass., 1963-1965; Mir, Moscow, 1978], Vol. 3.
19. A. V. Samsonov, *Space-Time Transformations of Electromagnetic Signals* (MEI, Moscow, 1997) [in Russian].
20. V. S. Chernousov, Radiotekh. Elektron. (Moscow), **10**, 1445 (1965).
21. K. A. Zakharov and M. I. Sugak, in *Proc. XXVIII Int. Conf. on Antenna Theory and Technology, Moscow, Sept. 22–24, 1998* (OAO Radiofizika, Moscow, 1998), p. 155 [in Russian].
22. N. V. Zernov and G. V. Merkulov, Zarubezh. Radioelectron., No. 1, 68 (1991).
23. M. G. M. Hussain and M. J. Yedlin, in *Proc. IEEE Intern. Radar Conf. RADAR-2000, Alexandria, USA, May 8–12, 2000* (IEEE, Piscataway, NJ, 2003), p. 263.
24. I. Ya. Immoreev and V. S. Chernyak, Radiotekhnika, No. 4, 3 (2008).
25. *Radio-Engineering Systems*, Ed. by Yu. M. Kazarinov (Vysshaya Shkola, Moscow, 1990) [in Russian].
26. V. G. Repin and G. P. Tartakovskii, *Statistical Synthesis under Prior Uncertainty and Adaptation of Information Systems* (Sovetskoe Radio, Moscow, 1977) [in Russian].
27. V. S. Chernyak, Radiotekh. Elektron. (Moscow) **24**, 2454 (1979).
28. H. L. Van Trees, *Detection, Estimation and Modulation Theory* (Wiley, New York, 1968; Sovetskoe Radio, Moscow, 1972), Vol. 1.
29. I. Ya. Immoreev and D. V. Fedotov, Radiotekhnika, No. 10, 84 (1998).
30. L. A. Bondarev, Radiotekhnika, No. 8, 33 (1981).
31. L. A. Bondarev, Radiotekhnika, No. 2, 24 (1984).
32. L. A. Bondarev, Radiotekhnika, No. 7, 8 (1990).
33. A. M. Brikker, N. V. Zernov, and T. E. Martynova, Radiotekh. Elektron. (Moscow) **45** (5), 559 (2000) [J. Commun. Technol. Electron. **45**, 510 (2000)].
34. *Fundamentals of Radar*, Ed. by Ya. D. Shirman (Sovetskoe Radio, Moscow, 1970) [in Russian].
35. Code of Federal Regulations, Title 47 Telecommunication, Part 15 – Radio Frequency Devices.
36. V. S. Chernyak, Radiotekhnika, No. 1, 18 (2008).
37. I. Ya. Immoreev and L. I. Telyatnikov, Radiotekhnika, No. 9, 33 (1997).